UNIVERSIDAD POLITÉCNICA DE MADRID

UNIVERSIDAD POLITÉCNICA DE MADRID

MÁSTER UNIVERSITARIO EN EFICIENCIA ENERGÉTICA EN LA EDIFICACIÓN, LA INDUSTRIA Y EL TRANSPORTE

TRABAJO FIN DE MÁSTER

Chemical, Physical and Mechanical Evaluation of Smart Cement-based Materials Incorporating Forest Biomass Ash

No REGISTRO: TFM MUEE ___/2019_

AUTOR: **SHAREEF OMAR**

TUTORA: **ANA JIMENEZ RIVERO**
ESCUELA TÉCNICA SUPERIOR DE INGENIERÍA AGRONÓMICA, ALIMENTARIA Y DE BIOSISTEMAS DPTO. INGENIERÍA AGROFORESTAL-UNIDAD DOCENTE DE CONSTRUCCIÓN

TUTORA: **ANA Mª GUERRERO BUSTOS**
INSTITUTE OF CONSTRUCTION SCIENCE EDUARDO TORROJA (IETCC-CSIC) AGENCIA ESTATAL CONSEJO SUPERIOR DE INVESTIGACIONES CIENTÍFICAS

TUTORA: **GLORIA PEREZ**
INSTITUTE OF CONSTRUCTION SCIENCE EDUARDO TORROJA (IETCC-CSIC) AGENCIA ESTATAL CONSEJO SUPERIOR DE INVESTIGACIONES CIENTÍFICAS

CONVOCATORIA: 2019
MADRID, JULIO, 2019

ACKNOWLEDGEMENTS

I would like to take this moment to thank my supervisors Dr. Ana Guerrero and Dr. Gloria Perez at Spanish National Research Council's Eduardo Torroja Institute of Construction Science (IETcc- CSIC) and Dr. Ana Jimenez at Technical University of Madrid for their help, support and guidance during my research, this work would have been impossible without them.

I would like also to extend my appreciation to the fellow group members at Eduardo Torroja Institute, and technicians at the Laboratory of Concrete as well as the Scanning Electron Microscopy Laboratory for being available and helpful during the experiments. They made my experience memorable.

Thank You.

Shareef Omar.

RESUMEN

La eliminación de las cenizas procedentes de la biomasa se convertirá en una preocupación real debido a la creciente adopción de la incineración y la cogeneración como uno de los tratamientos de residuos municipales y agrícolas. Por otro lado, la industria de la construcción utiliza una gran cantidad de materias primas, y el diseño de relaciones simbióticas con otras industrias en materia de residuos, subproductos o materiales secundarios es una idea atractiva en términos medioambientales. En esta investigación, se ha explorado el uso de cenizas de residuos de biomasa en la fabricación de materiales base-cemento con capacidad de "autoreparación", esto es, "materiales autorreparables".

Los materiales base cemento desarrollados y diseñados, contienen fibras que muestran la capacidad de fallar de manera dúctil con una capacidad de deformación entre el 3-7%, a diferencia de los hormigones comunes que son quebradizos y solo pueden producir una deformación del 0.01%. El desafío al fabricar estos materiales es que requieren un control estricto de las propiedades mecánicas, químicas y reológicas en la matriz para poder realizar la función de "autocuración". Es decir, la formación de gran número de pequeñas grietas con tamaño menor de 100 μm distribuidas por todo el sistema cementante, en lugar, de una grieta grande como se observa en otros materiales base cemento, se podrán sellar con el empleo de estos materiales. La presencia de las grietas a microescala puede facilitar y fomentar la entrada de compuestos corrosivos agresivos al material base cemento, como el ión cloro. El sellado de estas pequeñas grietas y posiblemente "curación natural" del material base cemento, mediante reacciones de hidratación del cemento y otras reacciones puzolánicas supondrá un aumento de las prestaciones mecánicas y durabilidad del material.

El objetivo principal de este estudio es evaluar el efecto químico, físico y mecánico de la adición de ceniza de biomasa forestal en materiales base cemento inteligentes (SCBM, del inglés *Self-healing cement-based materials*). El SCBM se ha formulado como un compuesto base-cemento de ingeniería autorreparable (ECC), en el que las cenizas volantes (CV) se sustituyen parcialmente por otros residuos, como es la ceniza de biomasa forestal (CBF).

Se han estudiado tres series: una serie de referencia (conjunto R) sin CBF, y dos series con diferente sustitución de CV por CBF, esto es, en una proporción CV/CF de 70/30 (conjunto A) y 30/70 (conjunto B). Se curaron durante 28 días a 98 ± 2% de HR y 20 ± 2ºC. Para evaluar la influencia de la adición de CBF en el material ECC, se realizaron estudios mecánicos y pruebas de absorción de agua capilar en muestras sin fisurar y fisuradas. Se han empleados dos tiempos de estudio: 28 días de curado y 28+28 días (28d de curado, y otros 28d para evaluar la recuperación)

Al finalizar el tiempo de curado, de cada serie se eligió un molde (3 probetas) donde se generaron grietas y otro molde sin generar grietas. La diferencia en el tamaño de las partículas y la composición de CV y CBF da lugar a efectos en la micro y macro-mecánica del hormigón. La conclusión principal de este estudio es que es posible sustituir parte de la CV en un material de

ECC con CBF y conseguir recuperación de prestaciones mecánicas y de durabilidad del material. Es necesario encontrar una proporción óptima de las cenizas que combine dos efectos positivos observados después de 28 días de recuperación la recuperación mecánica, como se ve en el conjunto B, con la absorción capilar estable, como se ve en el conjunto A.

Palabras clave:
Autoreparación, material base-cemento de ingeniería autoreparable, pequeñas grietas, cenizas de residuos de biomasa, rayos X, resistencias mecánicas.

ABSTRACT

The disposal of waste ash from biomass-based sources is bound to become a real concern due to increased adoption of incineration and cogeneration as a means of municipal and agricultural waste treatment methods. Construction, on the other hand, is one of those industries that use a large number of raw materials, and designing symbiotic relations with other industries concerning waste materials is an appealing idea in as far as environmentally conscious planning is concerned. In this research, we explore the use of biomass waste ash in the fabrication of self-healing engineered cementitious composites.

Engineered cementitious composites are fibre containing, cement-based materials that show an ability to fail in a ductile manner with strain capacity between 3-7 % unlike common concretes, which are brittle and can only afford a strain of 0.01%. The challenge in making these materials is that they require strict control of mechanical, chemical and rheological properties in the matrix in order to perform in a self-healing manner that is the formation of small, multiple cracks of less than 100μm throughout the system instead of one large crack as is observed in other cementitious materials. The availability of small cracks makes it easy for the composite to seal and possibly heal them naturally through hydration of cement and other pozzolanic reactions as cracks can encourage the entry of aggressive corrosive compounds like chlorine in the material.

The main aim of this study is to evaluate the chemical-physical and mechanical effect of the addition of forest biomass ash in new smart cement-based materials (SCBM). SCBM has been formulated as a self-healing engineered cementitious composite (ECC), in which fly ash (FA) is partially substituted by other waste, a forest biomass ash (FBA).

Three sets were studied: one reference sample (set R) without FBA, and two sets with a ratio of FA/FBA content of 70/30 (set A) and 30/70 (set B). They were cured for 28 days at 98±2% RH and 20±2ºC. To evaluate the influence of the FBA addition on ECC material, mechanical study and capillary water absorption test were conducted in uncracked and cracked specimens, immediately after cracking and after healing for 28 days.

The difference in particle size and composition of FA and FBA give rise to effects on the setting, as well as micro and macro-mechanics of the concrete. The principal conclusion of this study is that it is possible to substitute part of the FA in an ECC material with FBA. It is necessary to find an optimal proportion of the ashes that combines two positive effects observed after days of crack healing: mechanical recovery, as seen in set B, with stable capillary absorption, as seen in set A.

Keywords:

Self-healing engineered cementitious composite, microcracking, forest biomass ash, X-ray, mechanical strength.

CHAPTER 1: INTRODUCTION

1.1 Thesis motivation

The demand and use of cementitious based construction materials has been increasing around the world, unfortunately, these materials produce environmental impacts due to the production of raw materials such as cement and sand. These materials are also susceptible to the development of cracks which end up weakening and deteriorating the structure due to attacks from aggressive chemicals in the environment.

While the development of cracks is unavoidable, their nature in terms of size or how many cracks are formed relies on the choice of materials at the design stage. One of the parameters that control the size and nature of cracks is the use of properly sized fibres, their volume fraction compared to the matrix and the bond these fibres form with the matrix. The materials (cement, sand, fly ash etc.) one uses have an influence on the type of bond formed as well as the ability of the mortar to seal or heal the cracks. One specific type of these self-healing materials is known as Engineered Cementitious Composite (ECC), this material utilizes the micro-mechanical understanding of how short fibres used as reinforcement in mortars facilitate the formation of small but numerous cracks when faced with a mechanical load above its failure strength. These materials were developed at the end of the last century and they have already found applications in some countries.

As a way to further improve the sustainability of cementitious materials, there have been attempts to include recycled materials, when making concretes which helps to prevent landfilling. A good example is the replacement of part of cement with fly ash when making concretes which has been encouraged and is already standardized in most countries. Fly ash comes from coal plants which are being phased out in most developed countries as such there is a need to explore other options in this regard. Biomass waste ash is one of the alternative materials that would benefit if recovered in this way. A more interesting application is to use the biomass ash in a way that not only maintains the structural properties manifested by the original mortars but also aid in the improvement of advanced material responses.

CHAPTER 2: LITERATURE REVIEW

2. An overview of Engineered Cementitious Composites

2.1 Engineered cementitious composites

Engineered Cementitious Composites (ECCs) are a type of cementitious material that gives a ductile response when mechanically loaded. These composites, which contain short and discontinuous fibres, are specifically designed to form micro cracks when mechanically loaded above its first cracking strength instead of macro cracks as in most reinforced cement based composites. The ductile performance is found by carefully controlling the fibre type, aggregate texture, fibre volume fraction and the like, an important difference between the other fibre reinforced composites (cementitious) and ECCs is the fact that aggregates in ECCs are fine whereas other concretes possess course materials. These materials have a strain capacity that approaches as high as 3% in addition to possessing high tensile and compressive strengths that have seen them applied in the construction of bridges and repair of high-rise buildings as of date [1].

Another appealing aspect of ECCs is the effectiveness of self-healing in restoring mechanical properties of a composite. As has been previously mentioned these composites have mainly micro cracks with crack width lower than 100 μm [2], which makes it easier for them to be filled as the material undergoes autogenous healing. Autogenous healing here refers to the intrinsic ability of a cementitious material to close cracks due to the hydration of unreacted cement, formation of C-S-H gels and formation of calcium carbonates to mention but a few [3]; these mechanisms will be described later in more detail.

A formulation of self-healing ECCs has been proposed in the literature as based in high content of fly ash to enhance these autogenous healing mechanisms. Fly ash from different sources with pozzolanic and sometimes cementitious properties has found its way as a partial or full replacement of cement in concretes and similar composites albeit with stringent physical and

chemical requirements so as to be able to maintain structural capabilities of a cementitious installation.In table 2.1 we present the requirements imposed by ASTM Designation C 618 – 05 [4] wherein the minimum amount of Silicon, aluminium and iron oxides as well as fineness are stipulated.

Table 2.1. ASTM classification and requirements of fly ash for cement replacement [4].

Characteristic	Class N	Class C	Class F
Silicon dioxide (SiO_2) plus aluminium oxide (Al_2O_3) plus iron oxide (Fe_2O_3), min, %	70	70	50
Sulphur trioxide (SO_3), max, %	4	5	5
Moisture content, max, %	3	3	3
Loss on ignition, max, %	10	6	6
Fineness: Amount retained when wet-sieved on 45 μm (No. 325) sieve, max, %	34	34	34
Strength activity index: A With Portland cement, at 7 and 28 days, min, percent of control	75	75	75
Water requirement, max, percent of control Soundness	115	105	105

2.2 Design considerations of an Engineered Cementitious Composite

There are a number of factors that affect the performance of an ECC, ranging from the size of the particles, the fibre's mechanical and surface properties as well as composite preparation.

2.2.1 Fibre properties in ECC

The use of fibres in the making of structural composites has a long history; natural products like horsehair are believed to have been used in plasters during the famous Roman empire, although it's important to note that without treatment natural fibres face deterioration of mechanical

properties due to decomposition [6]. In the 1970s engineers started to realize how the fibre-matrix relationship affects the micromechanics of the whole structure through the generation of small but numerous cracks as long as the fibres were strong enough.

In the case of ECCs, PVA fibres are usually included in the mix and their surface chemistry affects how they behave in times of failure. As fibres with a hydrophilic surface, PVA tends to form hydrogen bonds with the cement in the matrix, which can be debonded if a shear force above a critical value is applied. Fibres contribute to the arrest of crack development as well as to stress transfer across the Composite matrix. Moreover, when the fibres and the bond connecting them to the matrix are strong enough, the material will be able to carry a load above the cementitious matrix's cracking load which helps it operate above the critical strain of the material without fibres. This behaviour leads to formation of sub parallel cracks of almost equal spacing as well as helping the usually brittle material display signs of plastic deformation in the stress - strain relationship. Such a, behaviour is mostly referred to as pseudo strain hardening [7]. It is important to remember that this behaviour is made possible when the critical tensile strength of the matrix is less than or equal to the fibre bridging strength.

2.2.2 Effect of random fibre dispersion and orientation on mechanical properties

When preparing the paste for an ECCs, it would be desirable that the fibres were well dispersed, and equally oriented in all directions in order to have isotropic mechanical responses, In reality, this does not happen and instead the flow of the paste during mixing will affect fibre distribution. Fibres at the top and bottom of a sample also tend to be almost aligned with the surface, as compared to the fibres inside the composite [8].

2.2.3 Snubbing effect and space between cracks in an ECC

The angle at which a fibre is inclined in respect to the applied load will affect how much force is needed to debond and pull out a fibre, and these will affect the length of the crack formed.

This phenomenon is called snubbing effect and its influence is stronger for the fibres that have a larger angle between them and the load [9].

Building on this knowledge, numerous researchers [9-10] developed formulas that help in prediction or development of fibre reinforced materials with preconceived properties. The spacing between cracks in a 3D sample that we can expect when loading an ECC is given by:

$$x'_3 = L_f - \sqrt{\frac{L_f^2 - 2\pi L_f \lambda x''}{2}} \qquad 1$$

λ is a crack reduction parameter due to discontinuous random fibres and is calculated as

$$\lambda = \frac{2(4+f^2)}{\pi(e^{fi2}+1)} = \frac{4}{\pi g} \qquad 2$$

L_f is the length of the fibre, f is the snubbing coefficient, which takes values between 0 and 1 and is found experimentally during fibre pull out tests, x' is the multiple crack spacing in continuous fibre composites [9] and is given by:

$$x' = \frac{E_m V_m \varepsilon_{mu} r_f}{2 V_f \tau_{eff}} = \frac{V_m \sigma_{mu} r_f}{2 V_f \tau_{eff}} \qquad 3$$

E_m,V_m,σ_{mu} ,ε_{mu} are elastic modulus, Volume fraction, stress and strain at failure of the matrix which is found from the stress-strain curve, respectively. V_f, T_{eff}, r_f are fibre volume fraction, effective interfacial bond strength as well as fibre radius. To debond a fibre from the matrix, it has

to first be displaced δ due to application of load P [10], Lin and Li [11] gave the following energy based formula for fibre debonding:

$$P_d = \pi\sqrt{(\tau_0\,\delta + G_d)\,\frac{E_I d_I^3(1+\eta)}{2}} \qquad 4$$

And the Pull out load was calculated to be

$$P_p\,(\delta, L) = \pi\,\tau_0\,(L - \delta + \delta_0)(d_f + \beta(\delta - \delta_0)) \qquad 5$$

Of which the size of crack after debonding is found as:

$$\delta_0(L) = \frac{2\tau_0\,L^2(1+\eta)}{E_I d_I} + \sqrt{\frac{8G_d L^2(1+\eta)}{E_I d_I}} \qquad 6$$

Moreover, the optimal length of a fibre for a proper micro-cracking response can be calculated by

$$L_{optimal} = \frac{d_f \sigma_f}{4gr} \qquad 7$$

The frictional bond is given by

$$\tau_o = \frac{P_b}{\pi d_f l_e} \qquad 8$$

Here, E_f is the elastic modulus of the fibre, d_f is the diameter of the fibre,

$$\eta = \frac{E_f V_f}{E_m V_f} \qquad 9$$

Le is the length of the fibre embedded in the matrix during pull out and G_d is the chemical bond strength

$$G_d = \frac{2(Pa - Pb)^2}{\pi^2 E_f d_f^3} \qquad 10$$

The loads Pa and Pb can be found experimentally in a single fibre pull out test, which gives a graph as the one below:

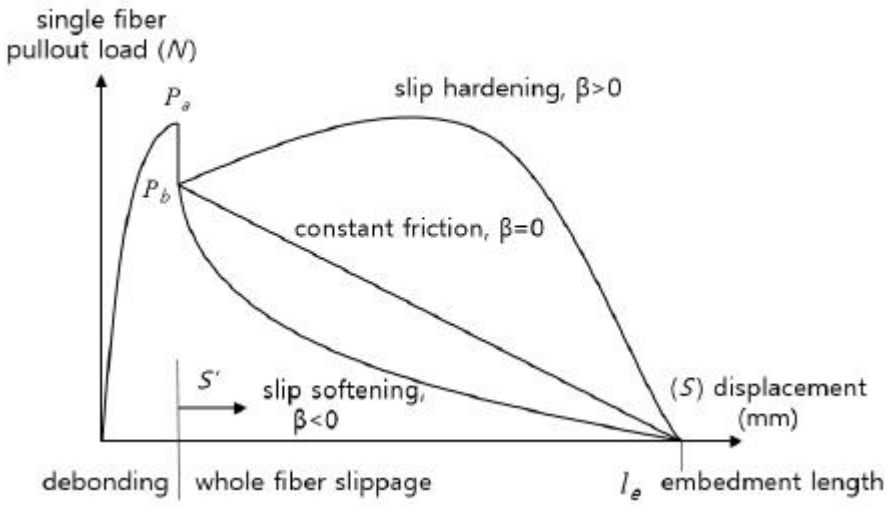

Figure 2.1. Fibre pull out test graph showing the loads P_a and P_b used in micro-mechanics design [11]

PVA fibres were found to have higher slip hardening effects due to abrasion and jamming which leads to better mechanical properties [11, 12].

2.3 Use of Fly Ash in cementitious composites

As has already been discussed, fly ash is being used as a replacement in cementitious composites in civil engineering projects including in ECCs. Sahmaran and coworkers [13] probed the changes due to the use of fly ash in ECCs in place of cement. They found the composites possessed a small crack width, as well as small compressive and tensile strength at 28 days in comparison to high cement content ones. For a fly ash to cement ratio of 1.2, the sample had a crack width of 48 μm, 62.5 MPa compressive strength and 5.141 MPa tensile strength whereas the sample with 2.2 fly ash to cement showed a crack of 30 μm, 54.1 MPa compressive strength and 4.82 MPa in tensile strength [13]. An exhaustive research by Victor Li [14] noted that the replacement fly ash should not have a higher proportion of amorphous carbon as carbon accumulates around the fibres, leading to lubrication during pull out. On the contrary, this is not entirely an issue when the carbon content is low since it removes the need to lubricate the fibres with oil during processing.

The other observation that should be considered when using fly ash is that one of the reasons for success of PVA fibres in ECC comes from their affinity to hydration products in cement like $Ca(OH)_2$. In fly ash however, the Calcium ions are not free, so its addition reduces the chance of bonding between fibre and matrix, a situation that leads to low values of chemical bond (G_d) [13].

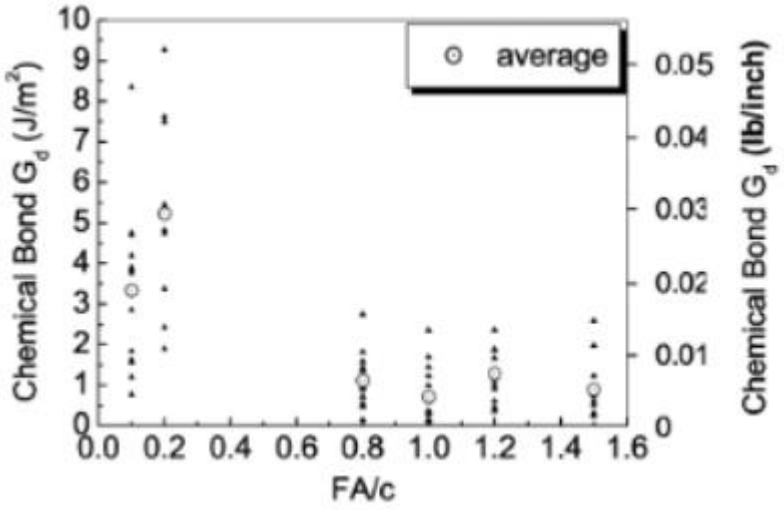

Figure 2.2. Low chemical bond of PVA fibre to matrix at high fly ash content [12]

The formation and propagation of steady state cracks is also affected by an ECCs fracture toughness, elastic modulus, volume fraction of the fibre as well as by the chemical bond.

The matrix toughness J_{tip} is supposed to be lower than the complementary energy J_b for an ECC to get steady state microcracks.

$$J_{tip} \leq \sigma_0 \delta_0 - \int_0^{\delta_0} \sigma(\delta) d\delta \equiv J_b'$$

11

The complementary energy is higher when the bond is low, and it favors a higher frictional bond τ_o

$$J_b' = V_f \frac{L_f}{d_f}\left(\frac{\tau_0^2 L_f^2}{6 d_f E_f} - 2G_d\right) \quad (12)$$

J_{tip}, the matrix toughness can be found by

$$J_{tip} = \frac{K_m^2}{E_m} \quad (13)$$

Where K_m is fracture toughness and E_m is the elastic modulus of the matrix. A ratio between J_b to J_{tip} can help predict a mixtures strain capacity as shown in the graph at figure 2.3. It is important to note that multiple cracking starts at $\frac{J_b}{J_{tip}} > 1$, which in this case is reached when FA/c to cement ratio is at or above 0.8

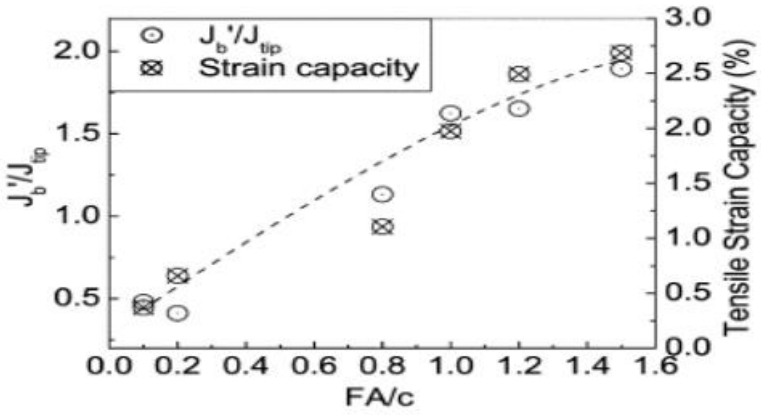

Figure 2.3. Ratio of fracture toughness to complementary energy in FA/C system and strain capacity [12].

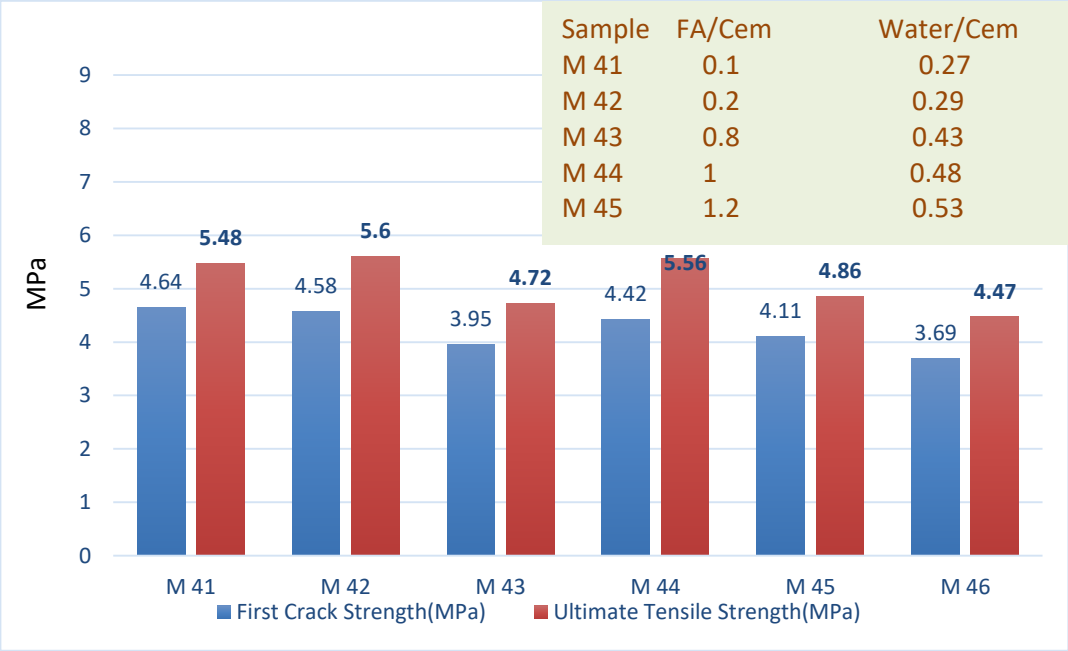

Figure 2.4. The relationship of fly ash -cement ratios to the tensile and compressive strengths [13, adapted].

In summary, an ECC made of fly ash differs to one without due to the differences in the chemical bond strength, this partly originates from the difference in the concentration of free Al^{+3} and Ca^{+2} ions which are prevalent in cement. These ions create an interface with PVA fibres whereas when fly ash content is increased, the ions' concentration drops which leads to lower a chemical bond formed with PVA. The multiple cracking in a fly ash containing ECC starts when the FA /CEM ratio reaches 0.8.

2. 4 Use of Biomass ash as a Supplementary Cementitious Material (SCM)

The disposal of waste ash from biomass-based energy sources is bound to become a real concern due to increased adoption of incineration and cogeneration as a means of municipal and agricultural waste treatment method. Construction is one of those industries that uses a large amount of raw materials, as such using the waste from power and waste management plants in building industry is an appealing idea in as far as environmentally conscious planning is concerned. Wood ash with a higher calcium content was found to be effective in replacing up to 15% of cement in concrete, by improving its compressive strength and leaching resistance in marine and freshwater environments [14]. As a replacement material, its contribution to microstructure and to the physico-chemical properties of concrete has largely been studied. Mortars that incorporate biomass ash were associated with reduced Alkali Silica Reactions where alkalis react with silicate compounds, which leads to expansion when the resultant gels absorb water [15]. Silicates are also important in cementitious composites as they form part of C-S-H gels which improve mechanical responses in materials, whereas alkalis are available in most biomass ashes due to processing methods that were used (eg. paper making) [15]. The works from different researchers have proven the ability of biomass ash to promote pozzolanic and hydration reactions, as well as a reduction of the Interfacial transition zone (ITZ) which is a poorly packed zone in concretes with a high porosity and weak mechanical properties. Sergio et al used nanoindentation to study the ITZ zone in an industrial sugarcane bagasse ash based cementitious composite, in addition to the improved workability of the paste , it was found that the zone was reduced by 70%. This effect was attributed to the small biomass ash particles, filling up the spaces and reordering the zone (wall effect) [16]. N. Kumar et al. [17] used rice husk biomass ash in combination with different additives like coal fly ash, silica fume, nanosilica and Metakaolinite. Other authors before [17, 32] have found the material showed improvements in regards to reduced chlorine penetration and alkali reactions as.

It was also observed that, in addition to physically filling up the ITZ, the blends with rice husk and assorted variations of additives all showed the presence of pozzolanic reaction products C-S-H in cases where coal fly ash was employed. Another major finding in this project was that the surface area of the composites is not the leading factor defining their mechanical properties as can be seen in the figures 2.5 and 2.6.

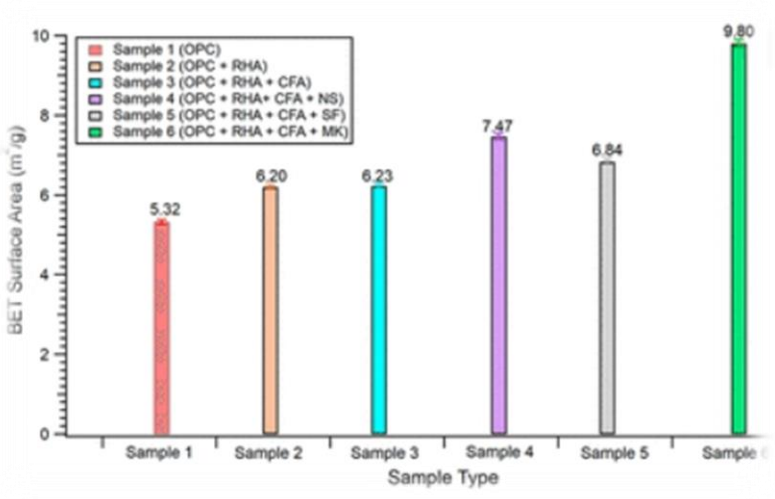

Figure 2.5. Effect of supplementary cementitious materials on surface area of cementitious material [17]

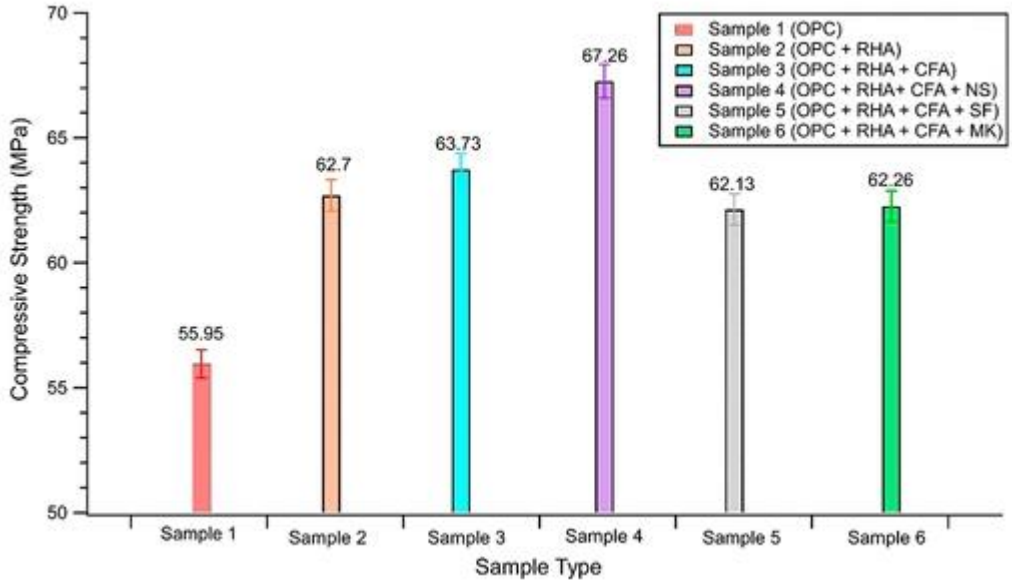

Figure 2.6. Compressive strengths of specimen with different supplementary materials [17]

We can observe from these graphs that a high surface area was not directly correlated with the highest mechanical properties, but rather additional features were in play [17].

2.4. 1 Rheological properties of Fly ash and Biomass ash admixtures

The use of admixtures of different size and response towards water and plasticizer affects the flow properties and workability of the paste, as well as the stability of the final composite. Park, Noh and Park [18] studied the influence of ground blast furnace slug, BFS (5962 cm^2 /g), fly ash, FA (3650 cm^2 /g) and silica fume, SF (200.62cm^2 /g) using rheometry.

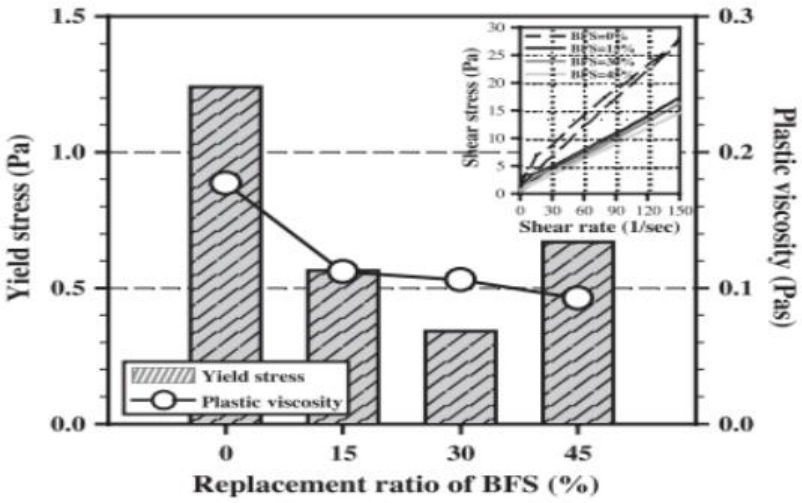

Figure 2.7. The relationship between the percentage of Blast Furnace Slag and rheological yield stress of the paste [18]

In BFS the yield stress of the paste dropped as the percentage of the slug was increased in the mixture, while his behaviour was reversed when 45% BSF was used (see the bars in figure 2.7). Thus the flowability improvements are encountered when a lower percentage of addition is used.

The authors attributed this improvement to the lower size of BSF particles as compared to cement, which lowers the friction during flow. Fly ash showed an increase in both shear and yield stresses as the amount of ash used was increased (see figure 2.8) due to adsorption of superplasticizer on carbon contained in fly ash [18].

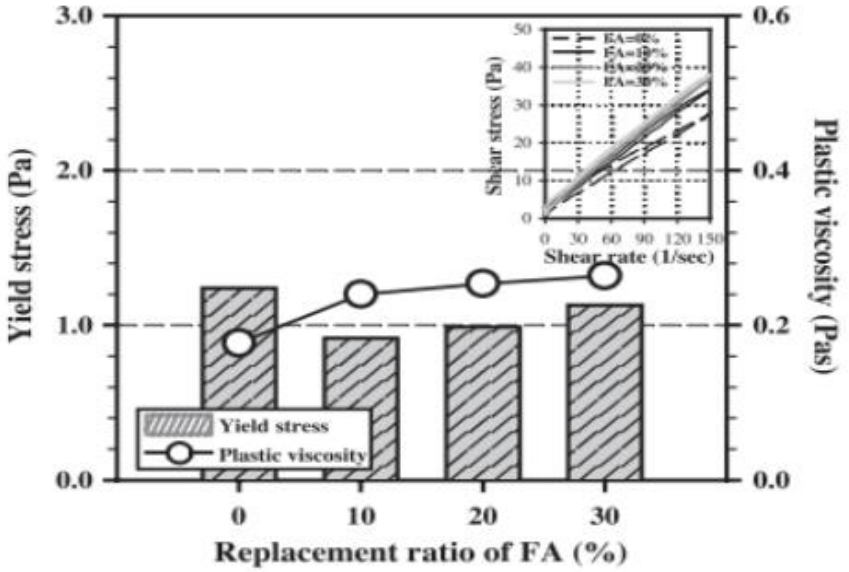

Figure 2.8. Effect of fly ash on rheological yield stress in paste [18]

In the case of ECCs, Li and Li [19] noted that the consistency of mechanical properties in the manufacture of Engineered Cementitious Composites is greatly affected by rheology, the type of mixers and admixtures used. These parameters have to be controlled in order to have a reliable set of mortars, even in cases where the formulation were kept constant as may be seen in figure 2.9.

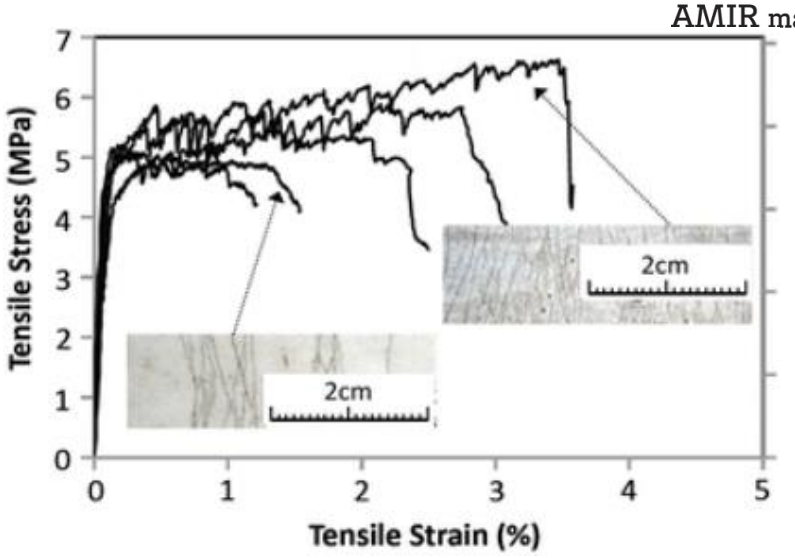

Figure 2.9. Variation of mechanical response in ECCs containing similar compositions [19]

Poor mixing capability leads to composites that have a side which did not receive proper fibre concentration to ensure strain hardening behaviour is observed, the lack of uniformity in the properties of the ECC can be a challenge when using the material in industry [19]. The researchers attribute change in viscosity through the use of Viscosity Modifying Admixture (VMA) to improved homogeneity and strain hardening behaviour as well as its consistency. As the percentage of VMA used in making ECC was increased, the composite showed a higher strain capacity in addition to a better consistency. Overall this research established that the best performance is obtained when 0.02% of VMA is used as can be seen in figure 2.10. This is also the amount that most researchers employ today in their research of Engineered Cementitious Composites. Water demand in cements containing supplementary materials also differs depending on the amount of biomass or fly ash that has been added usually due to the high specific area of these materials compared to cement [19].

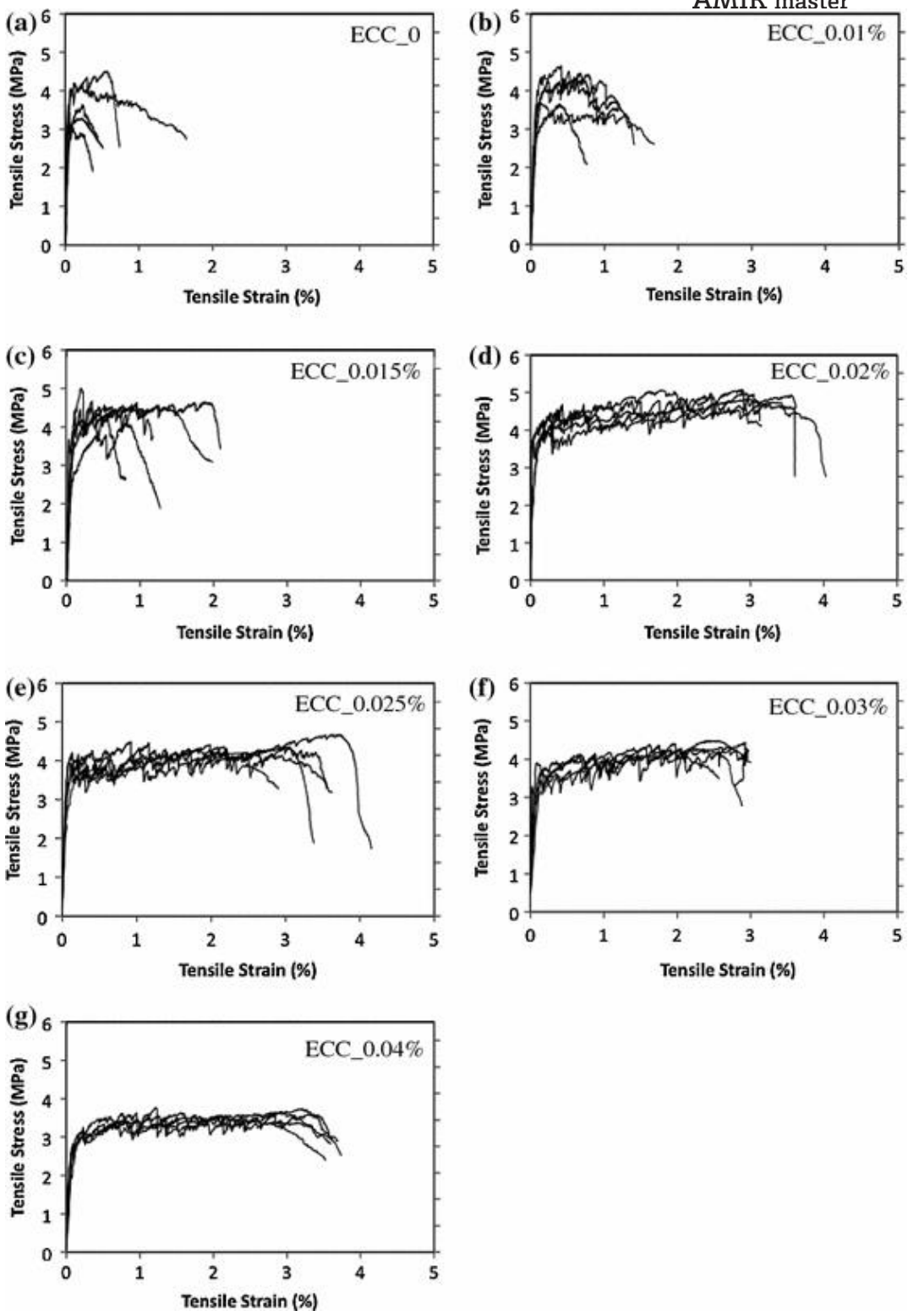

Figure 2. 10. Effect of superplasticizer on stability of mechanical response of the ECC [19].

2.5 Self-healing in Cementitious composites.

Cementitious composites have been known to possess an ability to heal themselves [20-22], evidence shows that the self-healing phenomena can be attributed to the formation of Calcium Carbonate in the reaction:

$$Ca^{2+} + 3\,H_2O + CO_2 \rightleftharpoons CaCO_3 + 2H_3O^{+} + 2OH^{-} \qquad 12$$

Where $Ca^{2+} + CO_3^{2-} \rightleftharpoons CaCO_3$ forms at pH higher than 8, whereas at water pH lower than 7.5, the material forms $Ca^{2+} + HCO_3^{-} \rightleftharpoons CaCO_3$. The sealing and healing process benefits also from physico-mechanical forces like swelling which make the crack smaller [20]. As the reaction shows, water or vapour is needed for the healing to occur, healing is also enhanced through the reaction of unreacted pozzolanic materials. In this part of the review, we are going to address the mechanisms involved in sealing and recovery of mechanical properties as well as the influence of fly ash on them. There are many ways to improve the self-healing in concretes that have been studied so far, these include incorporating microcapsules which contain chemicals or bacteria that promotes healing, shape memory alloys, and intrinsic healing encouraged by microcracks as is available in ECCs [21].

2.5.1 Inclusion of healing agents in the matrix

One of the main strategies for the inclusion of the healing agents in the cementitious matrix is the hollow tubes based or vascular strategy. As the name might imply, the material is embedded with hollow tubes (glass or porous concrete with coated walls) through which healing material is provided when a crack is observed. The tubes, connected either parallel or in network mode are designed to break with the formation of the cracks, and through this, they leak a liquid that improves the healing process.

For example, Dry used Methyl methacrylate liquid in order to reduce permeability in cracked concrete [20], while Mihashi utilised glass pipes containing non-diluted alkali-silica solution [20]. Figure 2.11 below shows the representation of the mechanism in this system with healing liquid dripping out of pipes at a crack.

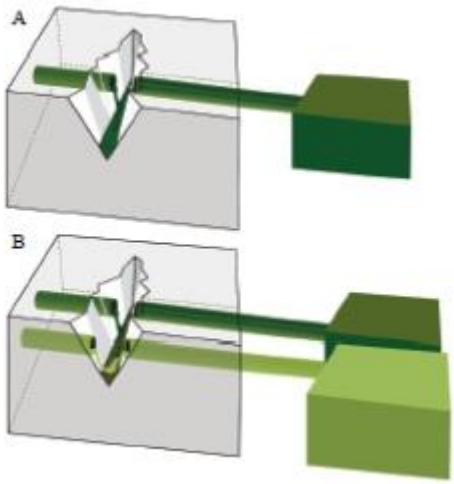

Figure 2. 11. Pictorial representation of self-healing system utilizing hollow tubes [20]

Some design of the pipes allow the refill of the healing agent once its depleted by making the tubes such that they are open to the surface [20].

Another form of design that encourages healing is by embedding microcapsule, which like the hollow tubes, fracture and release the healing agent they contain (e.g. adhesive) which aids in the healing process.

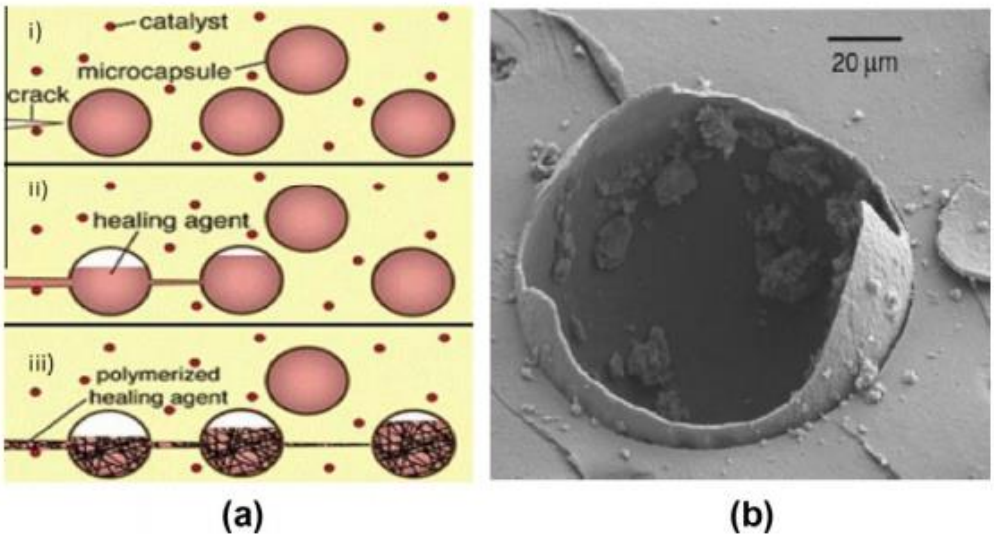

Figure 2.12. Microcapsules used in self-healing enhancement [20]

2.5.2 Self-healing through the control of crack size.

Unlike the two previously mentioned self-repair/healing techniques, where a healing agent has to be delivered in one form or the other, there is a way to rely on the natural mechanisms of pozzolanic reactions as well as the crack filling due to hydration products. The reaction products are not enough to fill large cracks, but are able to heal them when the cracks are small as in the case of ECCs. En Hua Yang and Victor Li came up with different attributes that can be used to assess the robustness of a self-healing system as summarized in the table 2.2 [21].

Table 2.2: Attributes of a adequate self-healing system for cementitious materials

Attribute	Characteristics
Pervasiveness	The system responds quickly to the cracking, the healing process begins as soon as the crack appears
Stability	The self-healing ability does not fade overtime, since structures are expected to last a long time
Economics	The prices are non-prohibitive to adoption in the construction industry
Reliability	Should be able to perform in different range of environments the material finds itself in
Repeatability	The material should be able to recover multiple times
Quality	Should maintain the physic-chemical properties that were present before the cracks

CHAPTER 3: MATERIALS AND EXPERIMENTAL METHODS

3. Materials and Experimental Methods

This chapter deals with the methods that were used to prepare and analyse the chemical, mechanical and physical characteristics of the Engineered Cement Composites in order to understand if specimen with different ratios of biomass ash formed an ECC and whether it was able to recover its mechanical properties after being loaded to fracture and developing cracks.

3.1 Characterization methods used

The raw materials were analysed in order to understand their physic-chemical properties. This was followed by a series of sample preparation and testing procedures, which will be discussed in this thread (table 3.1.).

Table 3.1: Summary of tests done in this research.

Test procedure	Characteristic studied	Sample	Days
Adsorption-desorption Isotherm: BET-N_2	Surface area of particles	Raw materials: Cement, Fly ash, Biomass ash. Different samples	Raw material 28days 28+28days
X-ray diffraction (XRD)	Crystalline phases	Raw materials: Cement, Fly ash, Biomass ash, different samples	Raw material 28 days 28+28 days
X-ray fluorescence	Chemical composition	Raw materials: Cement, Fly ash, Biomass ash	Raw material
Scanning Electron Microscopy	Imaging of samples microstructure	cured, cracked, and healed samples	(i) After 28 days of curing, (ii) after cracking by flexural loading, (iii) after 28 days of healing.
Energy-dispersive X-ray spectroscopy	Elemental analysis	cured, cracked, and healed samples	(i)After 28 days of curing, (ii) after cracking by flexural loading (iii) after 28 days of healing
Thermal analysis (TG / ATD / DSC)	Decomposition or formation of phases	Raw materials: Cement, Fly ash, Biomass ash	Raw material
Flexural test	Mechanical response, flexural strength	Cured and healed samples	(i)After 28 days of curing, (ii) after 28 days of healing
Compressive test	Mechanical response, compressive strength	Cured and healed samples	After 28 days of curing, after (28+28)
Capillarity test (Water permeability)	Crack closure, susceptibility to attack by aggressive chemicals	cured, cracked, and healed samples	(i)After 28 days of curing, (ii) after cracking by flexural loading (iii) after 28 days of healing

3.1.1. Adsorption-desorption N_2 Isotherms: BET-N_2 Surface Area

On the surface of a material, gases can be held due to a physical or a chemical bond that forms between them. This phenomenon is called adsorption and when the force involved is only physical, the process is called Physisorption, whereas when the material and gas are chemically bonded, it is called chemisorption. These phenomena are utilized in order to establish qualitative and quantitative properties of a material by measuring the pressure variation of a specific gas at constant temperature due to gas adsorption and desorption in the material. The common gases used to measure the so-called adsorption-desorption isotherms include Nitrogen, Argon and Krypton. One of the main properties established by this type of is the porous structure of materials. According to IUPAC, pores can be categorized into [24]:

I) Micropores: These are pores, which are less than 2 nanometers in diameter.
II) Mesopores: These pores range from 2 to 50 nanometers, and
III) Macropores: These pores are above 50 nanometers.

The quantitative analysis of N_2 isotherms used in this work is able to give the micro, meso and total pore volumes, the surface area, as well as pore size distribution by utilizing different models. The surface area of an adsorbent is related to the very first layer that is formed on the surface of a sample (the monolayer). This layer is usually formed at low relative pressures and the end of a monolayer can be noticed sometimes by the sudden uptick in the volume of adsorbed gas. The quantity of gas used to make this monolayer can be converted into the surface area of the adsorbent.

3.1.1.1 Brunauer–Emmett–Teller (BET) theory and Specific Surface Area

Based on the work done by Brunauer, Emmett and Teller (BET) the adsorbed gas can be modeled as

$$\frac{1}{\text{Vadsorbed}[(\frac{P}{P0})-1]} = \frac{1}{\text{Vmonolayer}*C} + \frac{C-1}{\text{Vmonolayer}*C}(\frac{P}{P0}) \quad 14$$

Here V is the volume of the gas; C gives a value that shows the extent of energy of adsorption in the monolayer, P/P_o is the relative pressure. The recommended range to construct a graph for this equation is between 0.05-0.35 P/P_o. This model results into Surface area (S_{BET}) given as;

$$SBET = a.\frac{poVm.NA}{R.273K} \quad 15$$

Such that

$$SBET = \frac{4.355}{\text{Slope}+\text{Intercept}} \quad \text{and} \quad CBET = \frac{\text{Slope}}{\text{Intercept}} + 1 \quad 16$$

Where *a* is the area of N_2 molecule which is equivalent to 16,2 $Å^2$ at -197.3^oC, V_M is the volume of monolayer and N_A is Avogadro's number (6.023 E23) [25].

3.1.1.2 Pore Volume

The pore volume is related to the volume of the adsorbed gas at specific sizes. Initially, the amount of gas adsorbed at micropores is obtained and from this value, the volume adsorbed in the mesopores can be calculated from the graph of adsorbed volume vs relative pressure (figure 3.1). The intercept is considered as the micro volume, while to get the meso volume the following formula is used:

$$Vmeso = Vtotal - Vmicro \quad (17)$$

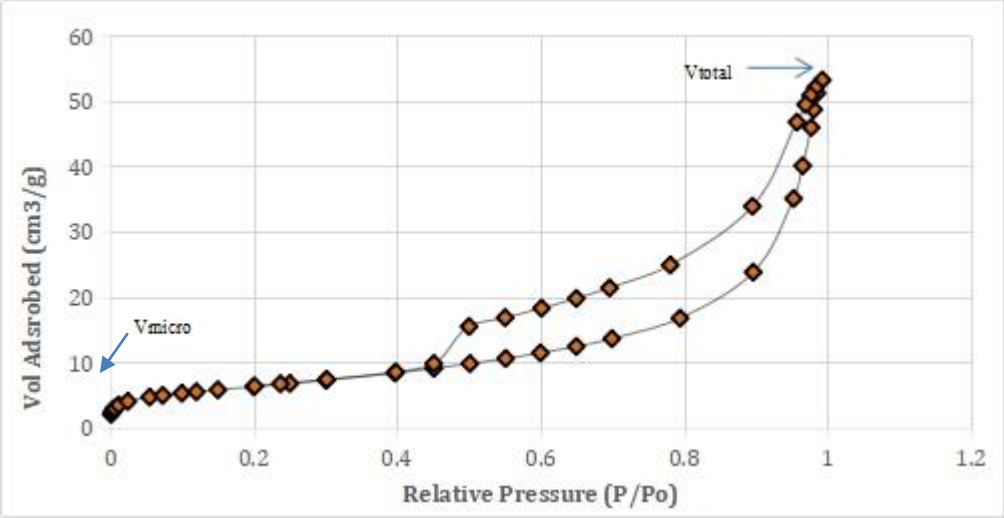

Figure 3.1. A graph of relative pressure (P/P_o) vs gas volume adsorbed (cm^3/g)

The obtained value is converted to Pore Volume (Standard temperature and pressure) by:

$$Vpore = \frac{\text{Mass N2}}{\text{Density(N2)}} \quad (18)$$

$$V_{pore\ (cm3/g)} = 1.5468\ V_{ads}$$

The mechanism involved in adsorption of Nitrogen gas in a sample results into characteristic graphs that help us properly understand the nature of a material, due to the hysteresis loops developed and the types of isotherms involved. The classification utilized in the scientific world was published by IUPAC. which divides the isotherms into six classes or groups, in addition to four distinct hysteresis loops [26] as can be seen from figure 3.2 below. The Isotherm I represents a material that is made of micropores, which leads to a graph that starts out steep at low relative pressures and quickly levels off in volume adsorbed vs relative pressure graph. This phenomenon

is attributed to a high adsorption potential generated from overlapping of potential energy between walls [26].

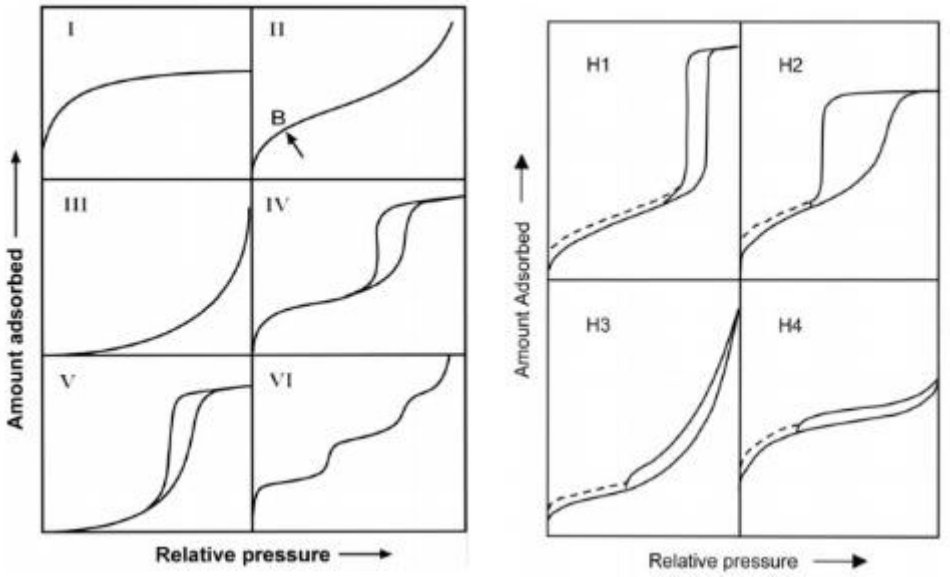

Figure 3.2. Isotherms (left) and hysteresis loops (right) in adsorption [26]

The isotherm II represents a completely reversible adsorption scenario where either a material has no pores or they are large (macropores). The Type III isotherms are also reversible, but unlike in type II, they have weak interaction between the gas and the material. The most relevant isotherm to us is type IV, in which the curve starts out as in Type II due to formation of a monolayer, followed by a multilayer, so that as the pressure rises, the gas condenses in the pores and the graph flattens. This is characteristic of mesoporous materials. Another important thing to observe here is the hysteresis loop formed, which also has different classification to be discussed later. Type V on the other hand starts out as in Type III but has similar ending to Type IV Isotherm. The hysteresis loops developed depend on the distribution and shape of pores. They range from H1 to H4 as can be seen in the figure 3.2. For cylindrical pores, the hysteresis observed is similar to the

one in H1, while H2 represents a material whose pores are not in a single defined form and H3 and H4 type hysteresis are found when a material has slit -shaped pores. The difference between them is that H4 is linked to the presence of micropores.

The isotherms obtained in this research resemble Type IV, with hysteresis loop H2, thus all our specimen are mesoporous, with disordered, but connected pores whose pore size distribution is uneven. The adsorption and desorption hysteresis loops join each other between 0.4-0.45 relative pressure at the lower end of the graph as is observed experimentally in most systems. This behaviour is associated with tensile properties of the liquid in the capillary [26-27].

3.1.2. X-ray fluorescence

The determination of the chemical composition of materials has been carried out conventionally by chemical analysis techniques, but nowadays more reliable results are obtained in the case of the inorganic materials in the field of construction by means of X-Ray Fluorescence (FRX). In this technique, the X-ray beam incident on the sample causes the expulsion of an electron from an inner layer of an atom (Figure 3.3). The gap is occupied by an electron of an external layer, emitting the energy difference between the two atomic levels in the form of a new X-ray photon, whose energy is different from that of the incident beam and is characteristic of the element in question. In addition, the intensity of X-rays of that energy emitted by the sample is related to the concentration of the element. In this way, it is possible to determine by means of FRX the elements that make up the sample qualitatively and quantitatively.

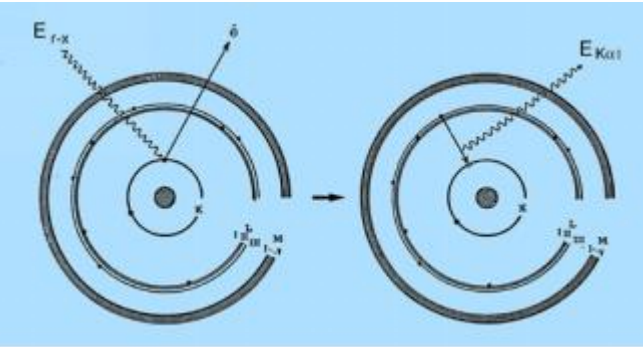

Figure 3.3. Scheme of the process that gives rise to the spectrum of X-ray fluorescence

The chemical composition of the raw materials and solid materials obtained throughout the research work is determined by this technique in an X-ray fluorescence spectrometer (WDFRX) model PHILIPS PW-1004, with a Sc-Mo X-ray generator tube. The specimen are prepared in pressed tablets, elaborated from 2 g of powder sample and 0.2 g of wax. The semi quantitative results of all specimen are shown normalized to 100%.

3.1.3. X-ray diffraction (XRD)

The X-ray diffraction (XRD) is one of the most used technique for the characterization of construction materials. It is based on the fact that X rays have a wavelength in the same order of magnitude as the interatomic distances in crystalline materials, which causes that when the radiation hits the material the result is the diffraction phenomena. The phenomenon can be described intuitively as a reflection of the X-rays in the crystalline planes of the material. One ray diffracted by a family of crystal planes will be obtained when the Bragg condition is verified:

$$n\lambda = 2d \sin 2\theta$$

Where:

λ is the wavelength of the X-rays employed

n is an integer greater than zero called the diffraction order

d is the interplanar distance of the considered family, and

θ is the angle of incidence of X-rays on the planes.

Different techniques are defined to measure the diffraction, depending on whether it varies λ or θ of the Bragg condition. In the field of construction, the most commonly used technique is powder diffraction, in which monochromatic light is applied to the sample and a sweep is made at angle 2θ to detect the diffracted beams in the different families of planes present in it. The angular

positions of the intensity peaks allow identifying the crystalline phases present in the material, for which the diffraction pattern of the sample is compared with the diagrams of known substances.

X-ray diffraction is a reliable method to determine which of the possible polymorphic forms of a substance are present in the sample, for example, $CaCO_3$ with calcite, vaterite or aragonite structure. It also allows differentiating between different oxides of the same metal more easily than in other methods. On the other hand, the intensity analysis of the peaks allows quantifying the relative proportion of each crystalline phase, although the reliable quantitative analysis is complex. The main disadvantage of this technique is that it does not allow the analysis of amorphous phases.

The XRD tests of this work are carried out with a Bruker AXS D8 ADVANCE diffractometer, whose X-ray generator tube uses a 3kW copper anode and a tungsten cathode. The radiation used is the Kα emission of Cu with a wavelength of 1.5405 Å. The voltage generating tube usually operates at 40 kV with a current of 30 mA. A sweep is made between 5 and 60 ° of the angular zone 2θ, with a sweep speed of 2°/min. For the identification of the different mineralogical species present in the specimen, the database of the Diffrac Plus EVA software is used.

3.1.4. Scanning electron microscopy (SEM) and dispersive energy analysis (EDX)

The scanning electron microscope is a powerful analysis tool, which allows the observation and characterization of materials and surfaces on a nanometric scale. The sample to be analyzed is irradiated with a focused electron beam that sweeps over its surface. Among the different types of signals produced when the electron beam collides with the surface of the sample, the secondary electrons and of the backscattered electrons are analyzed. Both signals vary following the differences in the topography of the surface and therefore provide an image of it.

Secondary electrons are low-energy electrons emitted by the atoms in the sample due to the impact of electrons in the incident beam. The emission of these electrons is confined to a volume close to the impact area of the incident beam, so that their analysis allows obtaining images of the topography of the surface with relatively high resolution and with good contrast thanks to the high number of electrons emitted. On the other hand, the incident beam causes the emission of

backscattered electrons, which are electrons that have been reflected by collisions with the atoms of the sample. They have more energy than the secondary ones and they have definite directions. The images of backscattered electrons are useful to distinguish between different types of materials, since the efficiency of emission increases with the atomic number of the element of the sample. In fact, elements with difference in their atomic numbers of only three units are distinguished by a good contrast in the image. In general, the backscattered electrons provide more complete and more interesting information than the secondary ones, but with lower resolution.

The potential of scanning electron microscopes is usually increased with the introduction of techniques that allow the compositional analysis of the sample. EDX (Energy Dispersive X-ray Spectroscopy) technique is typically introduced, which analyses the X-ray signal characteristic of the element that forms the sample and that are emitted by the impact of the electron beam. In this way, identification of materials and contaminants is possible, as well as estimation of relative concentrations of different elements on the surface of the sample.

The electron microscopy images of the present work are taken with a HITACHI S-480 microscope with a tungsten source and a BRUKER X-Flash 5030 detector was used for the compositional analysis by EDX. Both in the case of powdered samples and in monolith samples, a conductive adhesive is used for fastening to the metal sample holder and the surface is metallized with a carbon sheet

3.1.5. Thermal analysis (TG / ATD / DSC)

The term “thermal analysis” includes a series of techniques in which some physical parameter of the system is measured continuously as a function of temperature, which varies in a controlled manner.

Different techniques are defined according to the magnitude measured and the most used in the characterization of construction materials are: thermogravimetry (TG), differential scanning calorimetry (DSC) and Differential Thermal Analysis (DTA).

In the case of TG, the variations of the weight of the sample with temperature are associated with the decomposition or formation of phases. The magnitude of the weight change in each interval allows determining the composition of the sample taking into account the reaction that causes it. On the other hand, DSC and ATD measure the energy changes that occur when the sample temperature varies associated with mentioned reactions. These parameters have the advantage that they allow to differentiate endothermic and exothermic processes. In addition, the analysis of the obtained curves allows obtaining parameters of the material such as thermal conductivity, heat capacity or the heat of a reaction.

The combined use of TG with ATD or DSC is usual for the determination of the content of different cementitious phases, such as, portlandite, calcite or sulphates. It is also possible to determine the content of hydration water and non-evaporated and combined water in cementitious materials. As a disadvantage of these techniques, it may be cited the difficulty of separating the

contribution of some phases to weight losses, due to the overlapping thereof in the same temperature range.

The thermal analysis tests of this work are carried out with a thermo balance model SATQ600, Texas Instruments, to detect the variation of mass with a sensitivity of 0.1 μg and a maximum temperature of 1500ºC. Approximately 20 mg of sample deposited in a platinum capsule is used. The samples are heated from 23 ± 2°C to approximately 1000°C, with a heating ramp of 10°C min^{-1} and with a nitrogen flow of 100 ml/min.

3.1.6. Mechanical characterization

Mechanical tests done in this work can be grouped into two stages:

i- The primary tests that are done when the specimen finished a 28 days period in the curing chamber. These tests are used to quantify the materials´ flexural and compressive strength, which depends on a number of parameters like type of cement, used, water to cement ratio, cement to aggregate ratio, bond between the materials in the matrix, size of the aggregates. These sets of parameters are of special interest in the present study.

ii- The flexural tests done on the samples that had been cracked at 28 days of curing and returned to the curing chamber for another 28 days to allow self-healing and mechanical property recovery. This test is important as it informs of the level of healing achieved by specimen.

For comparative purposes, structural materials need to have their intrinsic properties defined. In this case, values from flexural tests are used to calculate the stress experienced in a material just before rupture (σ_{flex}), as well as the modulus of elasticity (E_{flex}).

Mechanical characterization in this work is performed with an INSTRON 8801 universal testing machine in figure 3.4.

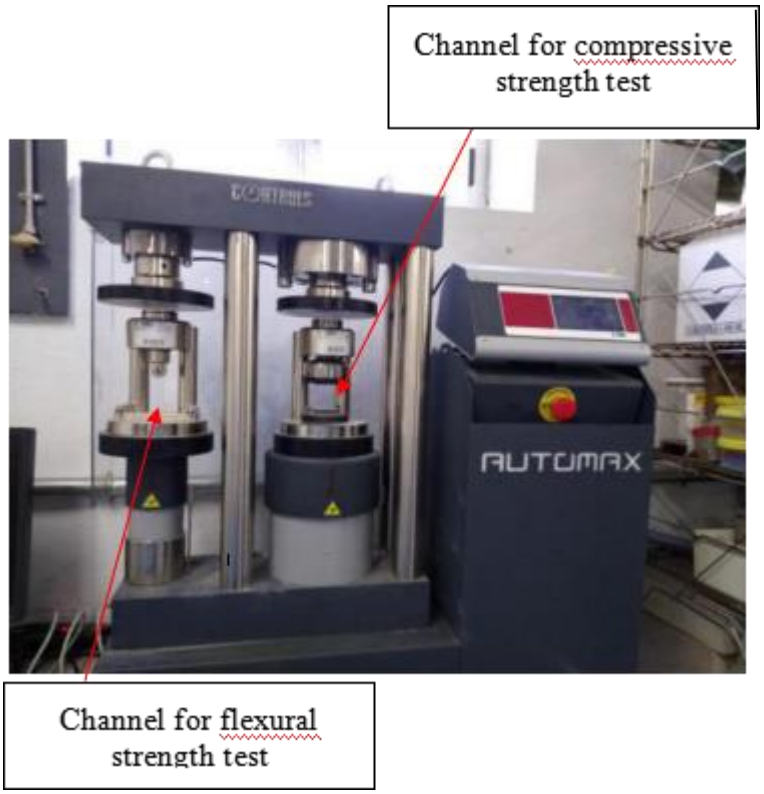

Figure 3.4. INSTRON 8801 universal testing machine used in this experiment

a) Flexural strength test: Three point bending test

The European standard for this procedure is EN1015. In this test, a 4cm x 4cm x 16 cm sample, supported at two ends, is pressed at the middle in order to compute the material's resistance to bending. The specimens were divided into two sets, as seen in figure 3.5. One group was loaded until fracture after curing for 28 days and was returned to the curing chamber in order to allow healing to take place while another was left in the curing chamber for 56 days (28+28d) in order to form a basis of comparison in terms of mechanical properties.

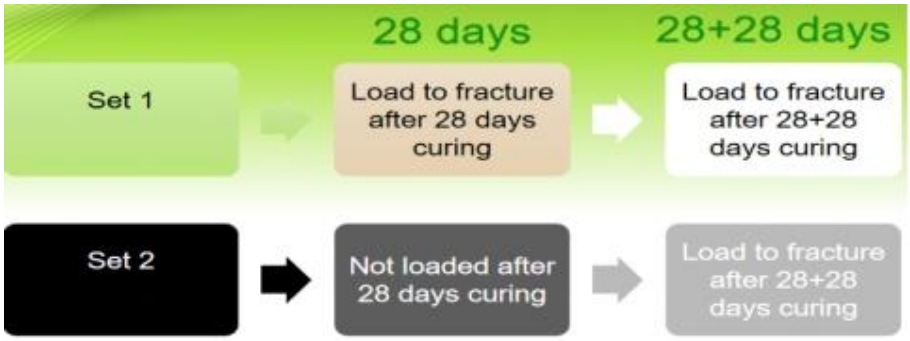

Figure 3.5. Schedule of mechanical tests

Flexural stress is close to tensile stress in most materials, so the three point bending test may be considered as an indirect tensile strength. The ratio between stress and strain in bending test is calculated using the formulas for flexural strength (σ_{flex} in MPa), elastic modulus (E_{flex} in MPa) and strain capacity (ε_{flex} in mm/mm) in bending test:

$$\sigma_{Flex}=\frac{3FL}{2bd^2} \quad 19$$

$$EFlex = \frac{L^3 M}{4bd^3} \quad 20$$

Where the following parameters are defined as per the pictorial representation of figure 3.6.

F load at a given point on the load deflection curve, (N)

L Support span, (mm)

m The gradient (i.e., slope) of the initial straight-line portion of the load deflection

D Maximum deflection of the center of the beam.

d Depth or thickness of tested beam, (mm)

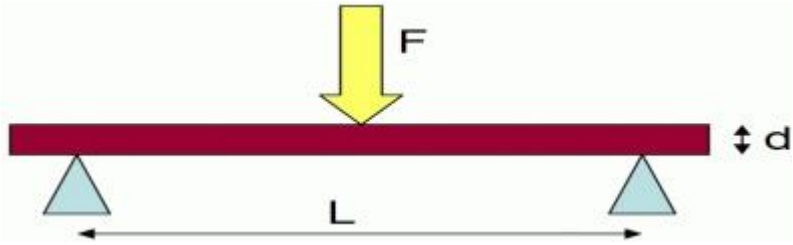

Figure 3.6. Pictorial representation of flexural tests

b) Compressive test

This test measures the stress a material can withstand (resist) when loaded in compression (see figure 3.7). The resulting value is important when classifying concrete materials since compressive strength is an intrinsic material property. The specimens involved in flexural tests were divided into two halves, and compressive tests were performed on these two pieces.

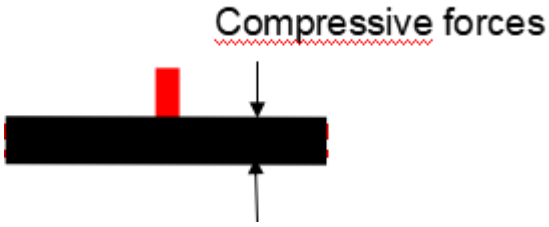

Figure 3.7. Loading in compression

3.1.7. Setting time of specimen

Setting time is the time a cementitious material needs to start losing its plasticity, and how long it takes for it to acquire some structural strength. The tests in this work were done by using the Vicat needle equipment in figure 3.8 to measure the initial and final setting time values, as defined in the ASTM C191-18a or UNE-EN 196-3:2017 standards. The initial and final setting times must be beyond 45 minutes and below 6.5 hours, respectively, for standard pastes.

Figure 3.8. Vicat needle machine

3.1.8 Transport Properties: Capillary Absorption test

This test measures the ability of mortars to take in water through capillarity, which is heavily

linked to the availability and size of cracks as well as to the porosity of the material. Capillarity is the flow of water in narrow spaces. In this experiment, cracked and uncracked specimen were put in an oven at 45°C for drying. Weight loss was recorded overtime until the difference in weight over a 24-hour period was less than 2%. The average drying time for all specimen was around one week. The specimen were covered all around with paint except the cracking face and its opposite (corresponding to the top and bottom faces during the three-point bending test), in order to restrict the water rise to only the bottom of the sample.

They were then put in a container filled with water covering up to 5 mm at the bottom as depicted in the schematic diagram given below. (Based on ASTM C642).

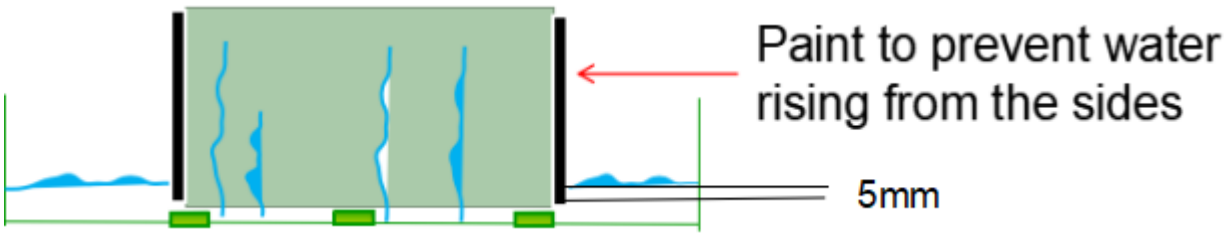

Figure 3.9. Design of capillarity tests

Weight gain was monitored periodically: The very first 5 minutes, then after 10 minutes, 20 minutes and so on. The amount of water (M) absorbed is theoretically linked to the sorptivity and the square root of time as given by Hall [25] by the equation:

$$M(t) = S\sqrt{t} \qquad 21$$

Where S is sorptivity and t is time. The absorption rate can be found by:

$$\mathrm{I} = \frac{\partial \mathrm{W}}{\text{Area of sample X } \rho} \qquad 22$$

∂W is the weight gain, the sample had 40 mm x 160 mm dimensions and the density of water was considered 1g /mm^3.

3.2 Raw materials

In these experiments, the following materials were used: sand, cement, superplasticizer, polyvinyl alcohol (PVA) fibres, fly ash (FA), biomass waste ash (industrial) (BA) and water.

The cement used in this work is an Ordinary Portland Cement (OPC) of the standard type CEM I 42.5R (figure 3.10), where 42.5 means that the material should have 42.5 MPa strength when compressed at 28 days, while R stands for rapid strengthening. Cement is manufactured from main materials as Limestone ($CaCO_3$) Alumina (Al_2O_3), Iron ore (Fe_2O_3) and silica (SiO_2) and it is usually mixed with Gypsum in order to control setting time..

Figure 3.10. General appearance of cement CEM I 42,5R

The fly ash used in this experiment was taken from Soto de Ribera thermoelectric power station situated in Ribera de Arriba in Asturias, Spain (figure 3.11 a).

Regarding the biomass ash used in this work (figure 3.11 b), it was forestal in nature and provided by a private entity.

a. Fly ash (FA) b. Biomass ash (BA)

Figure 3.11. General appearance of the ashes used in the experiment

Poly Vinyl Alcohol (PVA) fibres were chosen for this project (figure 3.12) for the reasons already expressed in detail in the literature review of chapter 2, which are their proper mechanical performance due to their interaction with the matrix. The fibres were 8 mm long and 0.039 mm wide and there was no surface treatment utilized. Some researchers have used oil as a lubrication liquid which helps during pull out and increases strain capacity, but since this research is at early stages, it was decided not to use lubricants. The density of the fibre was 1300 Kg/m^3, and its tensile strength was 1620 MPa.

Figure 3.12. General appearance of PVA fibres used in this work

Another important part of making an ECC is the choice of sand, particularly the size and

distribution. An ECC shows proper micromechanical behaviour when the sand aggregates are fine which helps amongst others to delay the fibre rupture during pull out. Taking this into account, 0.2 mm commercially sourced sand was used. (Figure 3.13).

Figure 3.13. General appearance of Sand used in these ECCs

To achieve a good flow as well as consistency in preparing mortars, a superplasticizer "MasterEase 3850" from BASF (Figure 3.14) was used at a constant amount of 1.5% by weight.

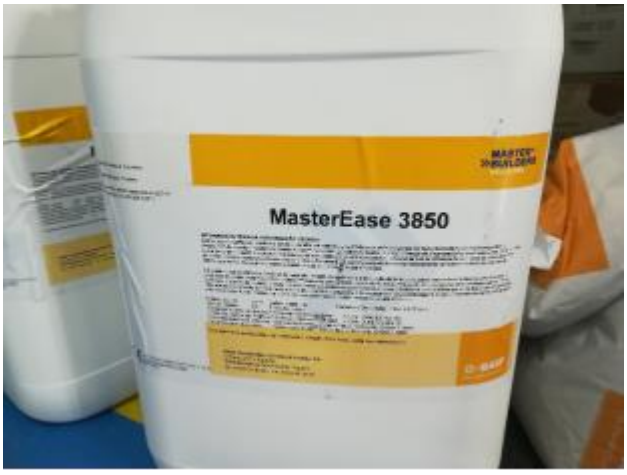

Figure 3.14. Superplasticizer used in these ECCs

3.3. Design of Formulations of Smart Cement Based-Materials (SCBM)

Three different formulations are studied in this work, named as R, A and B and detailed in tables 3.2. and 3.3. The reference formulation (R) reproduces the composition defined in the literature as the optimum for ECC with enhanced self-healing behaviour [21, 28]. The base of the mixture is formed by 432 g of cement and 518 g of fly ash, corresponding to a fly ash to cement ratio of 1.2, thus complying with the condition of being higher than 0.8 established in section 2.3. A total of 345.6 g of fine sand are added and the water to binder ratio is 0.35, being the binder the sum of cement and fly ash. A 1.5% of superplasticizer and a 2% of PVA fibres, which is an optimal amount for use in the reference sample as already referenced previously, are added to complete the mix.

As the main objective of the work is to characterize the new engineered cementitious composite that incorporates biomass ash, a partial substitution of the fly ash (FA) by biomass ash (BA) is proposed for the other two formulations. More specifically, formulation A includes 155.5 g of BA (with 362.9 g of FA) which represents 30% of the total ash in the sample and formulation B includes 362.9 g of BA (with 155.5 g of FA) which is 70% of the total ash content.

Table 3.2: The constant part of the mixture

Material	Content(grams)
Ordinary Portland Cement 42.5 R (CEMI 42.5R)	432.0
Sand (200 μm)	345.6
Superplasticizer	20.0
PVA fibres	26.0
Water (tap)	360.0

Table 3.3: Ash content in test specimen

Sample	Fly ash (FA) (g)	Biomass ash (BA) (g)
Reference	518	0
Sample A (30% Biomass)	362.9	155.5
Sample B (70% Biomass)	155.5	362.9

3.4 Mixing and curing

As seen in figure 3.15, the first step in the preparation of the ECC specimens is the mixing of the sand, fly ash, cement and, for specimen A and B, biomass ash in an automatic mixer for 15 minutes in order to make a dry homogeneous mix. This was followed by transferring the mixture into a Hobart planetary mixer. A solution of superplasticizer and water is poured slowly into the Hobart mixer while low speed stirring was in progress for 1 minute; the mixture was stirred further at an increased speed for two more minutes. PVA fibres were slowly dispersed in the mix under slow speed stirring in a manner that ensures homogeneous distribution of the fibre. This process on average takes 2.5 minutes, although the duration is not obligatory, rather the focus is on proper mixing. After fibre has been properly dispersed, the speed is increased and the mixer works at this new speed for 2 more minutes after which the paste is ready for moulding. The paste is poured into oil lubricated moulds, and manually compacted. The prepared specimen are

covered with plastic

film and left for 24 hours in the laboratory. The specimen are then removed from the mould, a process commonly known as demoulding, after which they are placed in a curing chamber with 98% humidity and 20 ^{o}C. Here they stay until time for mechanical or other tests are needed at specified days.

1. Dry mixing of cement, sand and ash

2. Automatic mortar mixer

Figure 3.15. Mixers used in the experiment

CHAPTER 4: CHEMICAL STRUCTURE AND COMPOSITION OF RAW MATERIALS

4. Chemical structure and composition of raw materials

The chemical contents of the specimen was found out using X-ray fluorescence, a technique that uses secondary X rays, which give characteristic properties.

4.1 Composition of Cement CEMI 42.5R

The cement used in this work was an ordinary Portland cement CEM 1 42.5 R, whose chemical composition is shown in table 4.1. The main component is calcium oxide with a percent content in weight of 63.73 %, followed by silica at 18.81%.

Table 4.1: Chemical composition of CEM I 42.5 R as obtained by X-ray fluorescence

Compound	Percentage (% weight)
CaO	63.73
SiO_2	18.81
K_2O	0.97
Al_2O_3	5.45
Fe_2O_3	2.58
MgO	0.75
SO_3	3.41
MnO	0.05
P_2O_5	0.05
Na_2O	0.06
TiO_2	0.23
SrO	0.05
ZnO	0.03
Cr_2O_3	0.01
Cl^-	0.02
PF	2.28

4.2 Composition of Fly ash (FA)

The main component of this ash (figure 4.1 and 4.2) was found to be Silica (SiO_2), which makes up about 46.4 % of the sample composition, followed by Alumina (Al_2O_3) which makes up 25.58% and Sulfur trioxide (SO_3) at 0.66 %. These percentages chemically qualify the fly ash as a pozzolanic material that is capable of partially replacing cement in the fabrication of a composite as already mentioned in Table 2.2. In this case, due to a combined Silica-Alumina content of above 70% and a Sulfur trioxide content of less than 4%, this FA could be classified as class F. A pozzolanic material, according to American Concrete Institute's (ACI CT-13), is a siliceous or silico-aluminous material that will, in finely divided form and in the presence of moisture, chemically react with calcium hydroxide at ordinary temperatures to form compounds having cementitious properties [14]. Other noticeable compounds in the fly ash composition include CaO (4.98 %), CO_2 (10.9%), Fe_2O_3 (4.9%), TiO_2 (1.33%) and MgO (1.03%). It is important to observe that the ash barely have chlorine (0.009%).

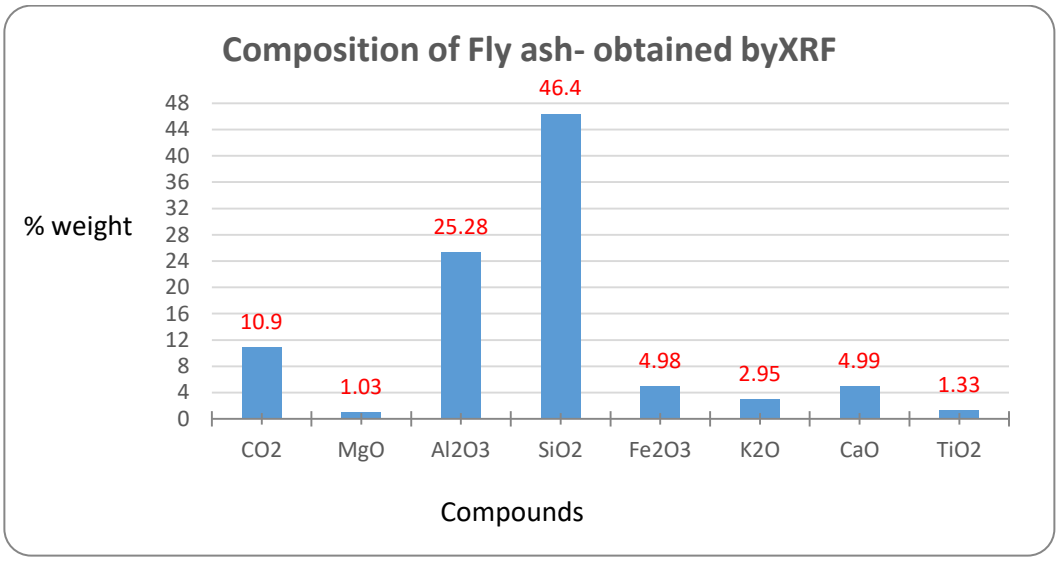

Figure 4.1. Main chemical components of FA used in experiment

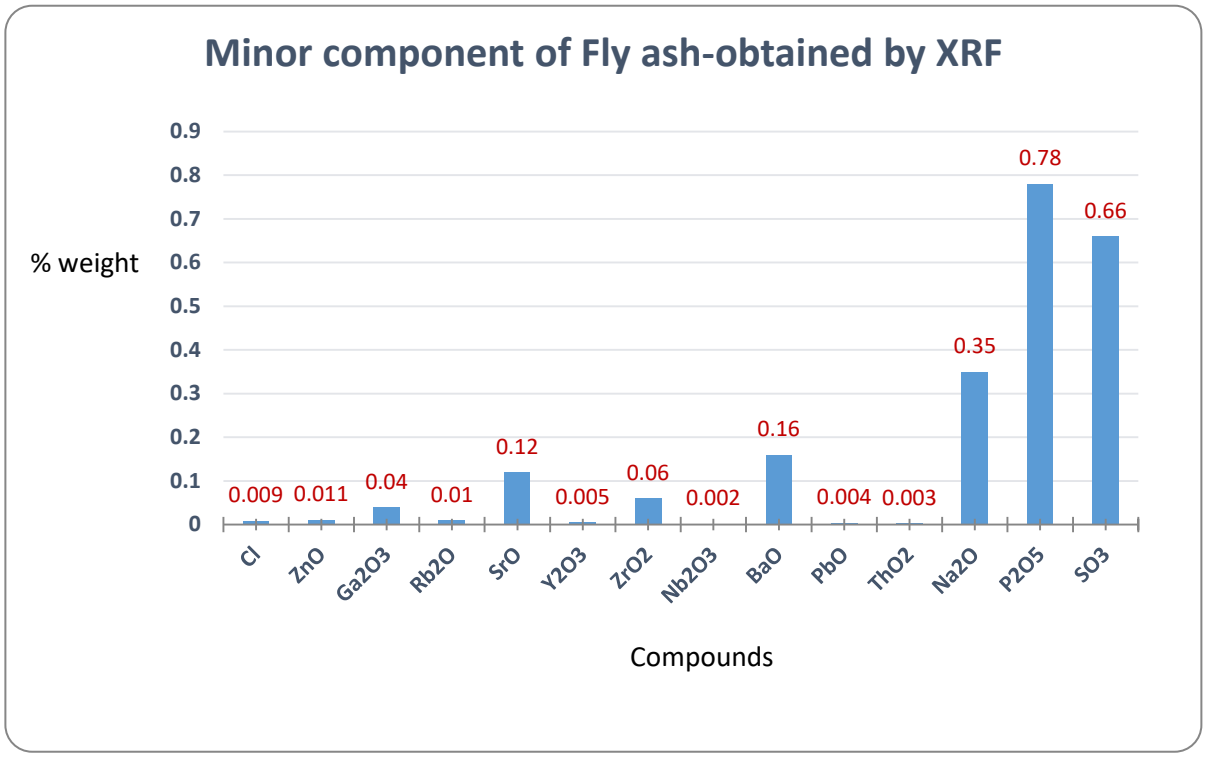

Figure 4.2. Minor components of FA composition

4.3 Composition of biomass ash (BA)

The most dominant chemical compound of the biomass ash (BA) (figure 4.3 and 4.4) is calcium oxide (CaO) at a weight percentage of 31.1%, while the content of Silica (16.9%) and Alumina (6%) are significantly lower as compared to fly ash (FA). The sulphur trioxide content, at 3 % is still lower than the limit given in ASTM C 618 – 05, CO_2 (12.8%), MgO (3%), and K_2O (5%) are found in a higher percentages when compared to the material they are intended to replace.

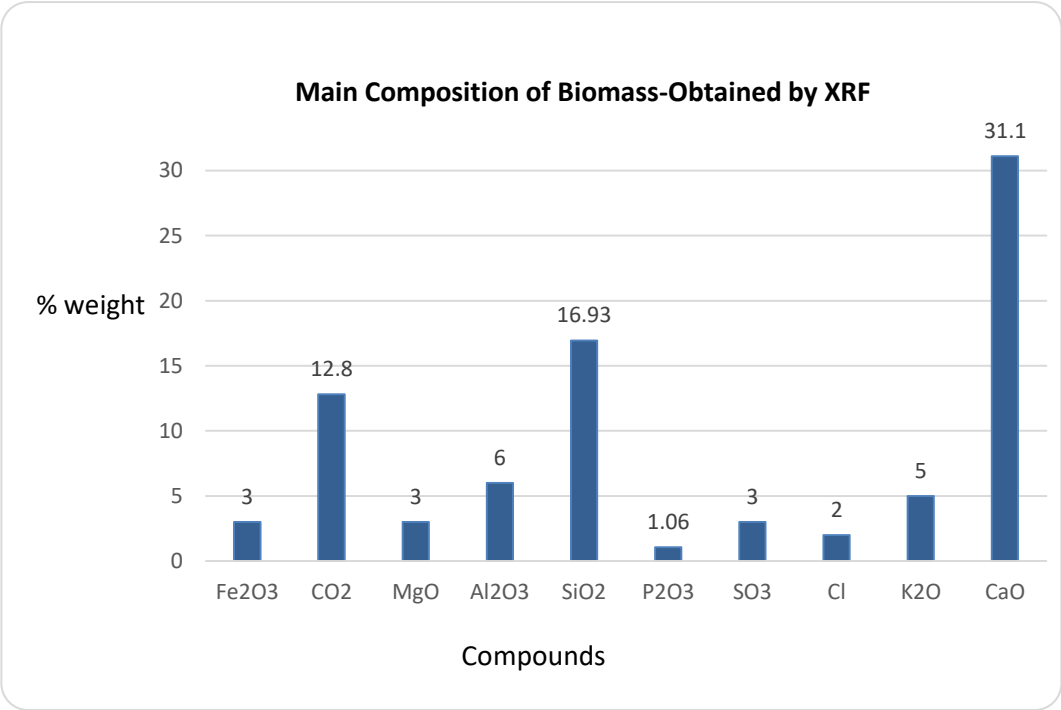

Figure 4.3. Main composition of BA

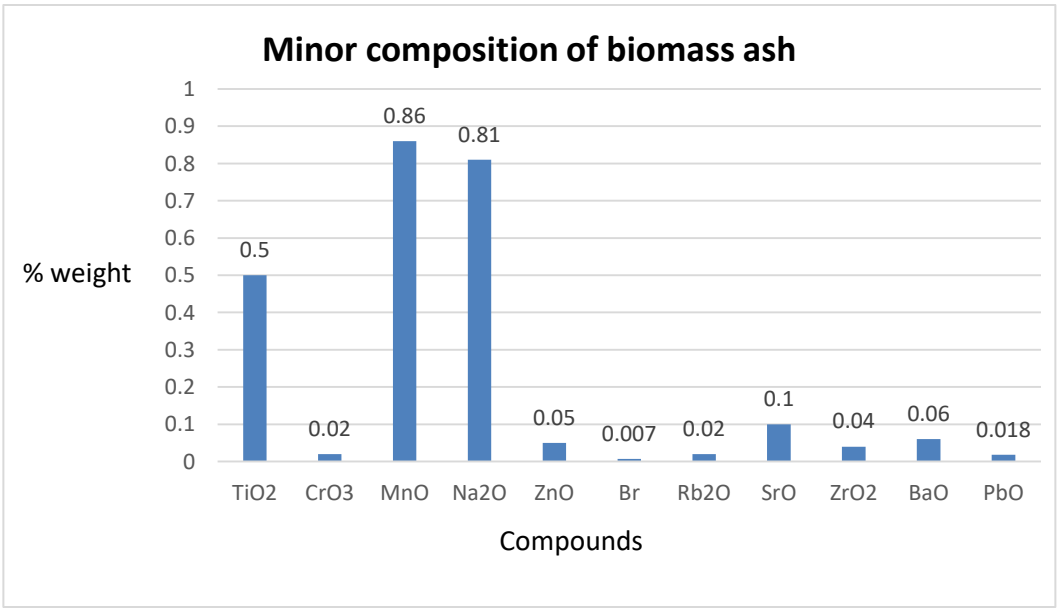

Figure 4.4. Minor composition of BA

Taking into account the compositional analysis results for fly ash and biomass ash, the final chemical contents corresponding to these admixture in the formulations R, A and B, with different amounts of biomass ash, are calculated. The content obtained for the main oxides and the chloride are depicted in figure 4.5. It is clearly observed that increasing the amount of BA in the mix gives rise to a decrease of the silica content that will probably reduce the effect of pozzolanic reaction, and of alumina content. In parallel, a clear increase of CaO content is observed for increasing BA proportion, being almost equal to the silica content in the B formulation. Finally, the estimated 1.4% of chloride content in this formulation must be taken into account in the analysis of the hydrated specimens.

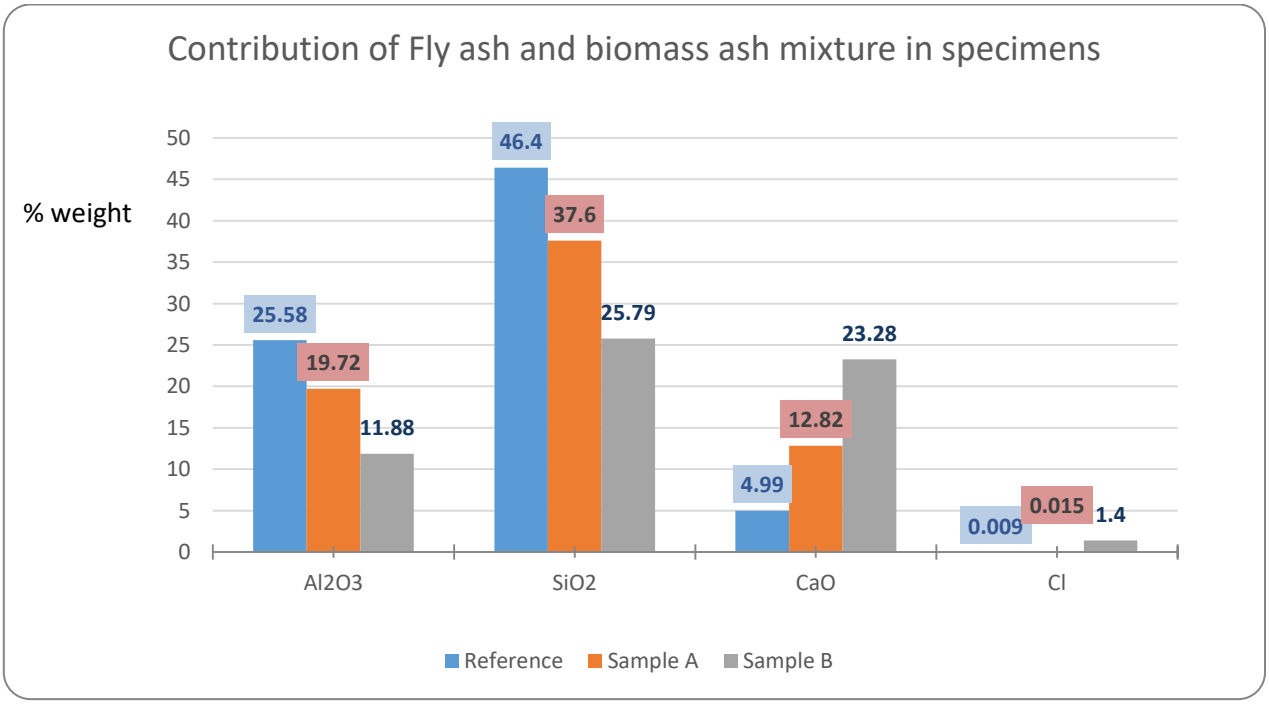

Figure 4.5. FA and BA contribution to the chemical composition of the matrix

4.4 X-Ray Diffraction: Crystalline phases in raw materials and Thermal Analysis

The X-ray diffraction patterns obtained for the raw materials are show in figure 4.6. As can be seen, as according to XRF results, FA has principally, mullite ($2Al_2O_3$ .SiO_2) and quartz (SiO_2) as its main crystalline phases, $CaCO_3$ was noticed amongst the present phases even though its crystallinity could be low. On the other hand, BA has as principal crystalline phases: quartz, portlandite ($Ca(OH)_2$), Sylvite (KCl) and Calcite ($CaCO_3$). In this point, it is interesting to comment the lower crystallinity of FA, with low intensity peaks on a wide amorphous halo in the diffractogram, as compared to BA. This different crystallinity of both ashes is expected to influence the behaviour of FA and BA in the ECCs explored in this work.

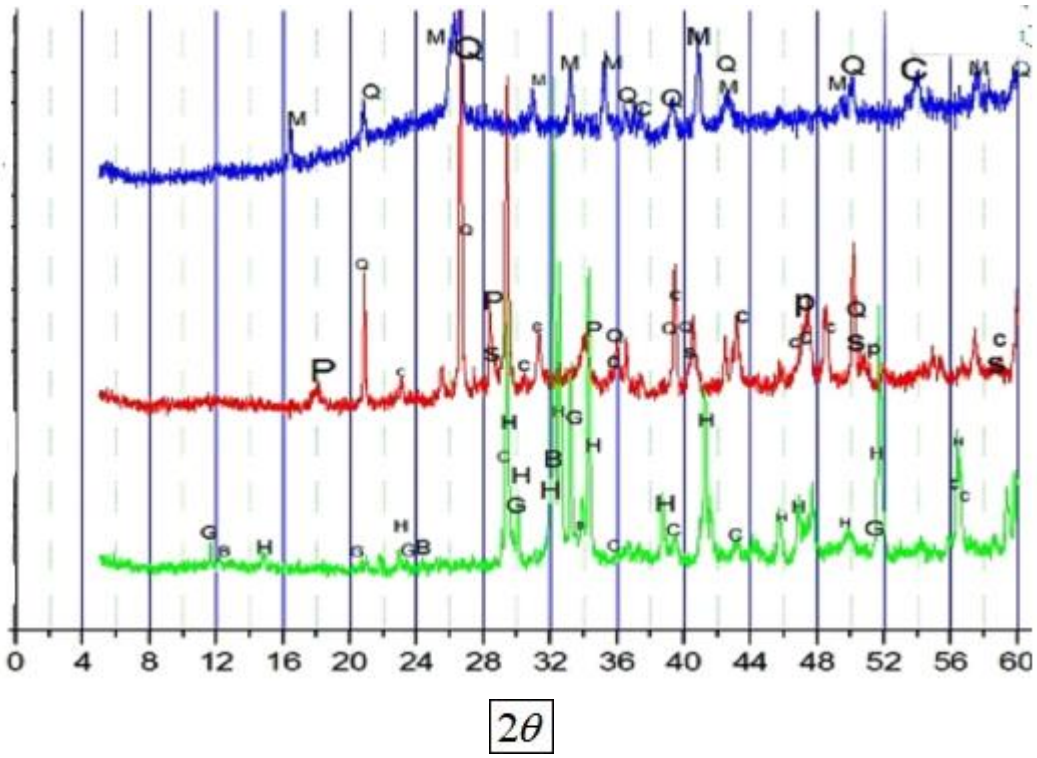

Figure 4.6. X-Ray Diffraction patterns of raw materials: green is for cement, blue is for fly ash and red for biomass ash: M=mullite ($2Al_2O_3$ .SiO_2), Q =quartz (SiO_2) G=gypsum($CaSO_4.H_2O$) P=portlandite ($Ca(OH)_2$), A=Ca_3SiO_5 B=$Ca_2Al_2Fe_2O_5$, S= sylvite (KCl), C= $CaCO_3$.

The figure 4.7 shows the thermogravimetric analysis of both ashes, FA and BA. The graph shows the weight loss of the respective specimen as a function of temperature (ºC). Fly ash does not lose two much weight overall the analysis due to the fact that it is mostly made of mullite ($2Al_2O_3 .SiO_2$), quartz (SiO_2) and hematite (Fe_2O_3) phases which do not undergo dehydration or decarbonation.

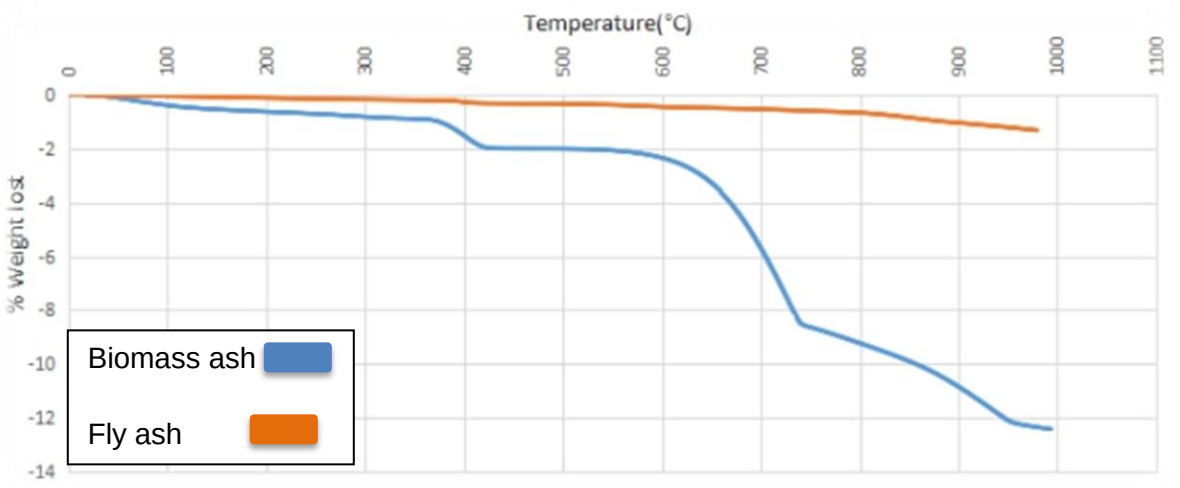

Figure 4.7. Thermogravimetric Analysis results of fly ash (FA) and biomass ash (BA)

With the loss of weight at different temperatures, the principal components of BA can be quantified. At temperatures between 300-500^oC, losses in inorganic compounds can be attributed to Ca $(OH)_2$, 500-700^oC loses are likely from $CaCO_3$ .And around 800^oC upwards from KCl, NaCl and the like. Table 4.2 below summarizes these details for the biomass ash.

Table 4.2. Weight loss (% by weight) in Biomass ash

Compound	Temperature (ºC)	Percentage lost (% weight)
$Ca(OH)_2$	300-500	1.41
$CaCO_3$	550-785	7.9
KCl	785-996	4.3

4.5. Scanning Electron Microscopy and Energy Dispersive analysis (EDX)

Figures 4.8and 4.9 show the microstructure of fly ash (FA) and biomass ash (BA). It can be observed that the specimen are not homogenous.

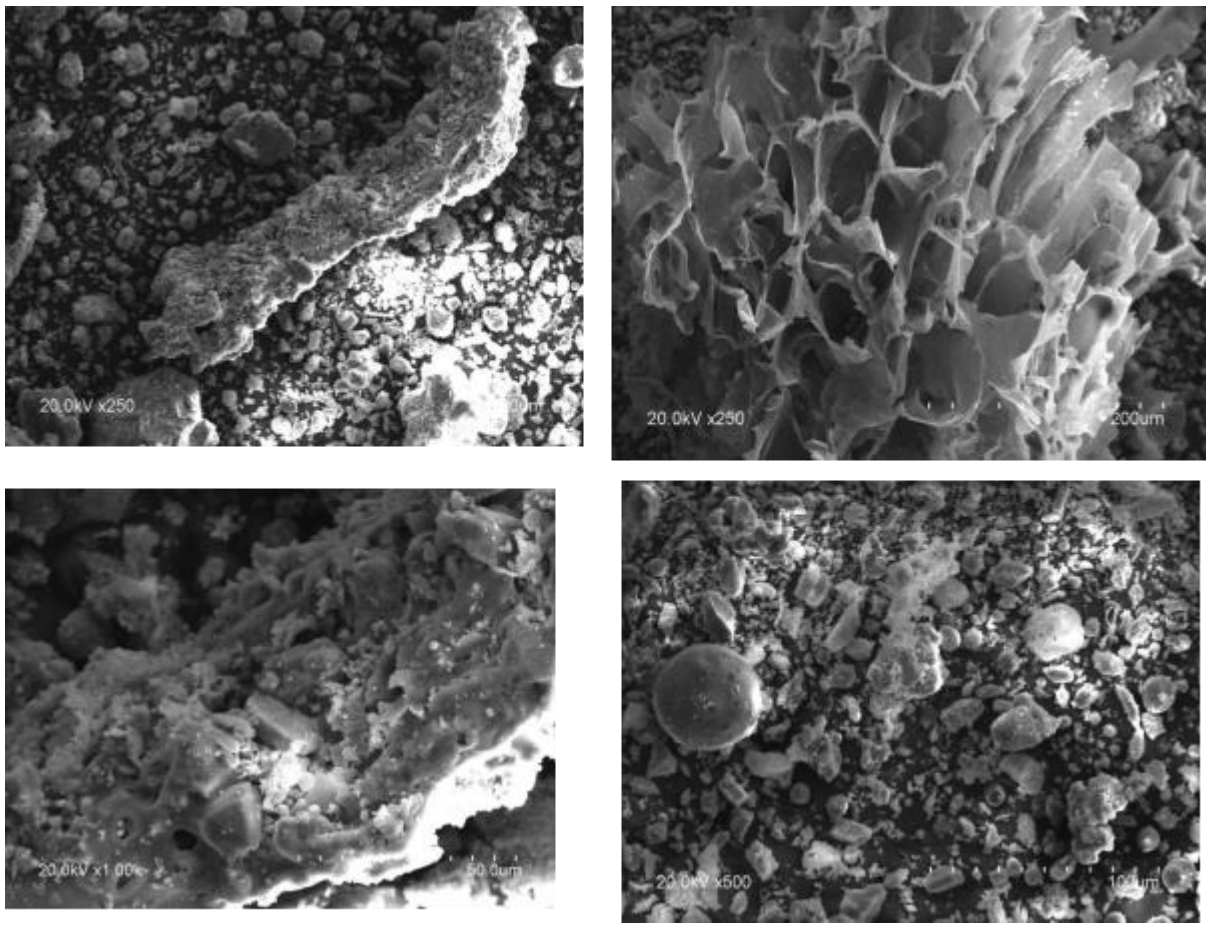

Figure 4.8. SEM images of the biomass ash used in the experiment

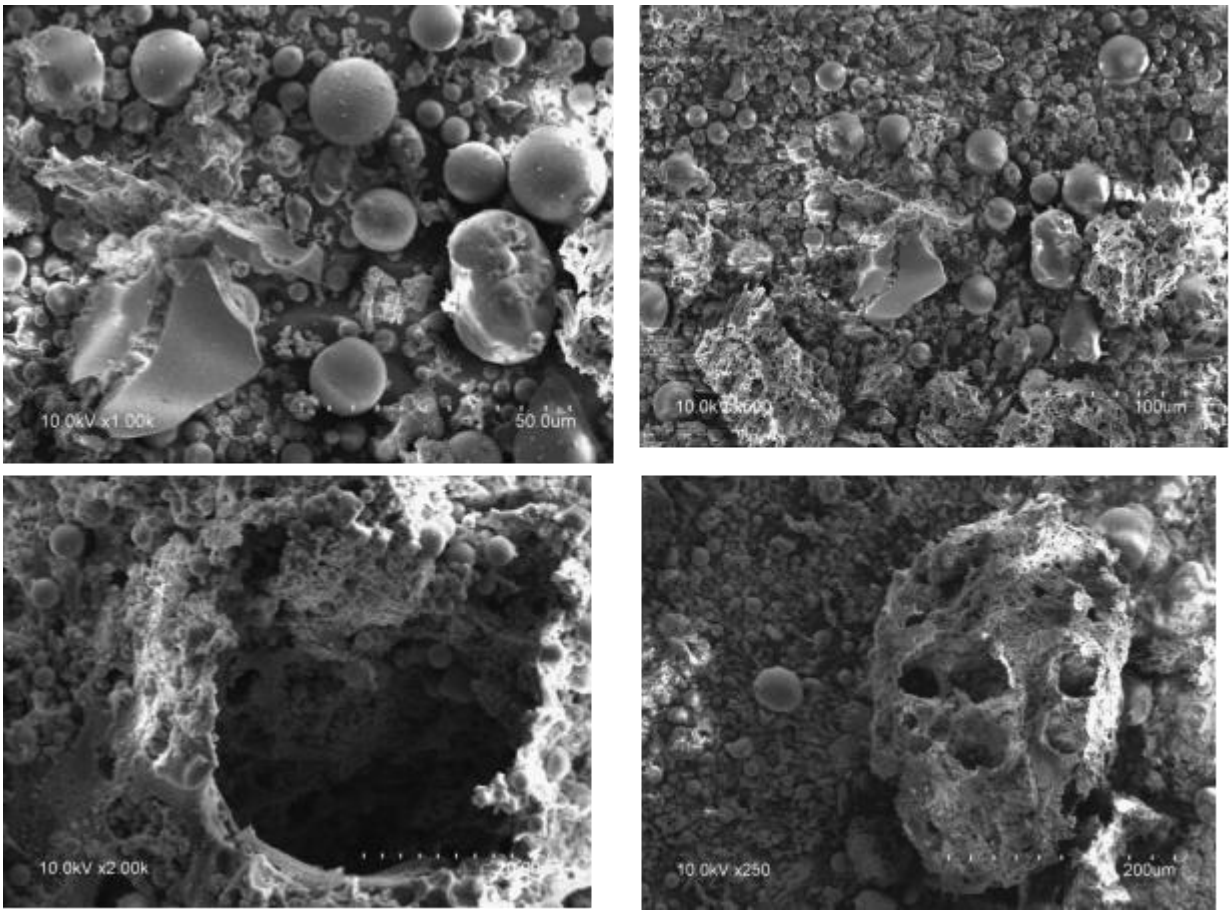

Figure 4.9. SEM images of the fly ash used in the experiment

The principal difference between the results shown in the two figures is that FA has more cenospheres with different sizes and a smooth surface (see the image in top left position in figure 4.9). In the case of BA, the microstructure is more heterogeneous. Only a few cenospheres may be observed and having a rough surface, that will have influence in the behaviour of BA in samples .

Summary of raw materials

The analysis of the raw materials indicates that the ordinary Portland cement used in this work has 63.73 % CaO as the main component, followed by 18.81% of SiO_2. The FA is mostly made of SiO_2 at 46.4%, followed by Al_2O_3 at 25.58%. The composition of BA, which is intended to replace FA in the sample, is dominated by CaO (31.1%) and SiO_2 at 16.93 %. FA shows a low crystalline character, being its main crystalline phases mullite ($2Al_2O_3.SiO_2$) and quartz (SiO_2) and a microstructure dominated by cenospheres, whereas in BA a more crystalline character is observed, with more variety of phases including Portlandite ($Ca(OH)_2$), quartz (SiO_2), calcite ($CaCO_3$) and sylvite (KCl).

Two important things should be noted from these results:

i) CaO is associated with early concrete strength due to hydration; this process also leads to retraction of the material, which can lead to cracking. A possible effect may then be expected due to the higher concentration of lime in BA.

ii) CaO or SiO_2, in addition to Al_2O_3, react to form hydration products, like ettringite or C-S-H gel, the latter being responsible for the mechanical behaviour of cementitious materials. These reactions take place at a later stage in the case of a material where part of cement is subtituted by FA or by a mix of FA and BA so that this could imply a different mechanical and durability response. In summary, the presence of FA and BA is expected to have an important role in the recovery of performance of ECCs studied in this work.

CHAPTER 5: RESULTS AND DISCUSSION

5.1. Evaluation of Mechanical and Transport Properties of Smart Cement-Based Materials (SCBM)

5.1.1 Mechanical behaviour of SCBM

Flexural and compression tests were performed on the samples based on Spanish and European standard UNE-EN 196-1. Figure 5.1 shows the mechanical properties: averaged flexural and compressive strength of samples of smart cement-based materials (SCBM) at 28days of hydration. As can be observed, the reference (R) containing fly ash only had the lowest flexural strength values, 8.9 MPa versus 10.2 MPa for A sample and 9.6 MPa for B sample. For compressive strength, a similar behaviour is observed, 67.3 MPa for reference versus 76.1 MPa and 73.2MPa for A and B sample, respectively.

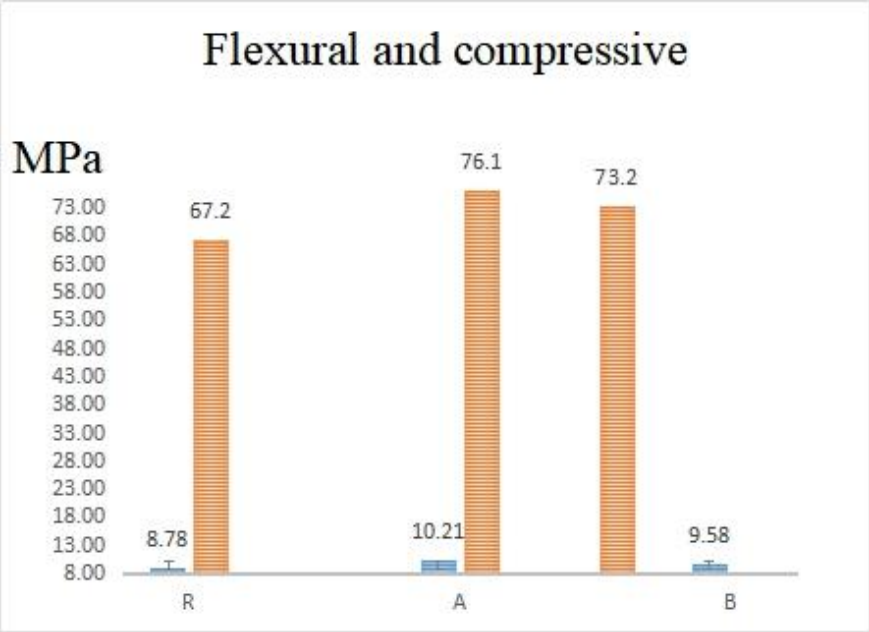

Figure 5.1. Flexural and compressive resistance of ECC samples at 28 days

The lower mechanical behaviour of R sample at early age of 28d is a well reported phenomena in fly ash substituted cementitious materials, due to the slower reaction kinetics of this addition [12].

However, it should be mentioned that the values obtained are higher than those found by Wang and Li shown in figure 2.4. On the other hand, the lower resistance values of R sample as compared to biomass rich samples, A (30% of BA) and B (70% of BA) are due to fewer hydration products contributed by fly ash and suggest a more efficient hydration of biomass ash at early ages. Another contribution that has been reported in the literature as affecting the development of mechanical resistances in cementitious materials is the particle size of the additions. The BA has a larger surface area (3.87 m^2/g) compared to FA (3.25 m^2/g). This parameter improves the compressive and flexural strength of the material through the formation of highly compact composites since the small particles are able to fill up the interspatial zones and other pores available.

Regarding mechanical performance of ECCs, a research by Wang and Victor Li [12] found that the use of high fly ash volume reduces the interface bond between the complex and the PVA fibre inclusions [12-14]. While Sahmaran and Li [13] attributed the decrease in strain hardening in high CaO ashes to the flexural strength observed in sample A may be attributed to the fact that it carries more CaO, the matrix toughness and chemical bond should be higher (to be explored in future work) whereas in B the increased biomass ash did not derail the strain hardening too much at least at the ages of 28 and 28+28 days.increased toughness and chemical bond formed with the fibres. With this idea in mind the improved

To evaluate the capacity of mechanical recovery of samples R, A and B, the flexural strength (Fs) values are studied at 28+28d, this is after 28 days of healing. As can be seen in figure 5.2, a higher increase of Fs for uncracked samples is observed for the reference formulation, with an increase of 8.20% with respect to 28 days.

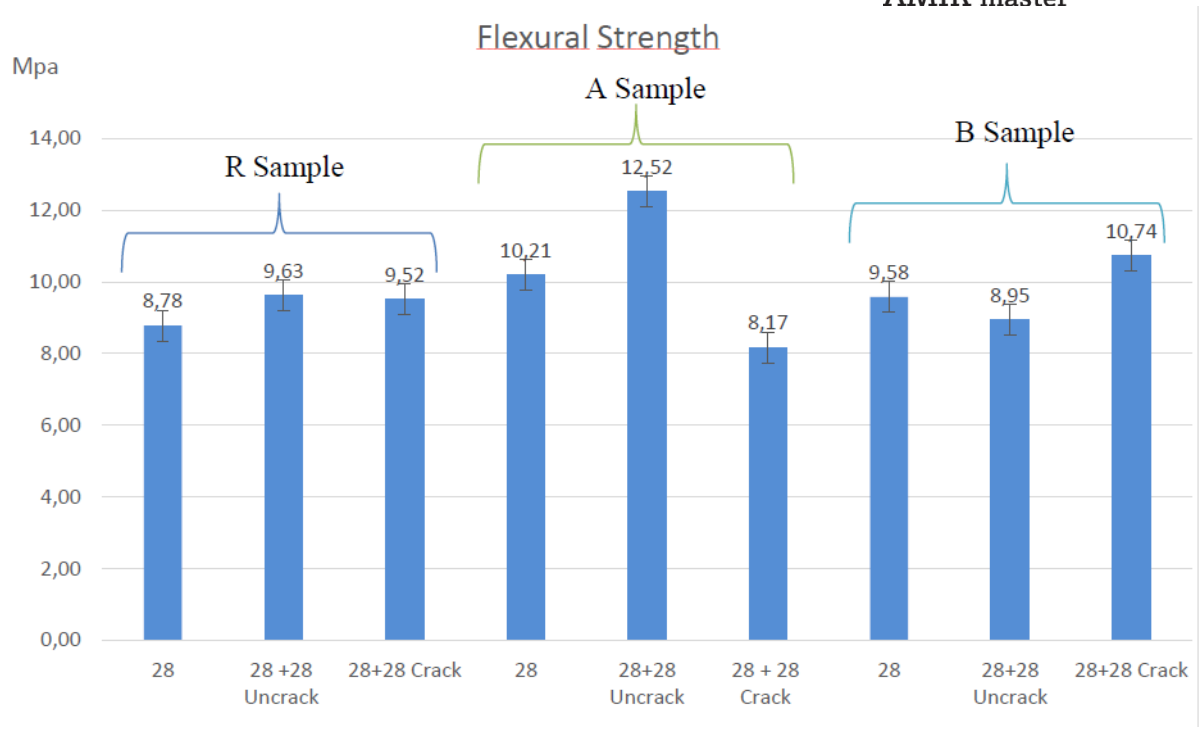

Figure 5.2. Flexural resistance of ECC samples at 28+28 days where their healing capacities are compared.

The tests at 28+28 days showed agreement with the literature which predicts much improved mechanical properties for fly ash containing composites due to enhanced pozzolanic reactions, which form C-S-H gels.

On the other hand, the results showed that each ECC formulation has a different behaviour in terms of recovery. In the R samples, it is observed that, the specimens cracked at 28 days and cured for 28 more has almost similar Fs values compared with uncracked specimens, indicating a complete mechanical recovery. Something similar occurs in B, in which the Fs for the cracked and healed specimens is even a bit higher than for the uncracked sample. However, sample A shows a worse capacity of mechanical recovery after 28 days for healing as the Fs value for the cracked specimens (8.2 MPa) is a 24% lower that the value for the uncracked ones (10.8 MPa).

5.1.2 Evaluation of transport properties: Capillary water absorption

Figures 5.3, 5.4 and 5.5, show the mean curves of mass increase (water absorption vs time0.5) of the specimens during the capillary water absorption test at 28 days and 28+28 days of self-healing and Figure 5.6 collects the values of the mean capillary water absorption coefficient ($K(kg/min^2 min^{0.5})$).

The uncracked and cracked specimens of reference material (figure 5.3 (a)) at 28d showed a similar mass increase until the end of the test. At 2 days of testing, cracked samples have an inverse behaviour, but over time, the behaviour is very similar. After 28+28d (figure 5.3 (b)), both samples have a similar behaviour and the mass increase is lower than the samples at 28d, due to the advance of hydration of the material.

.

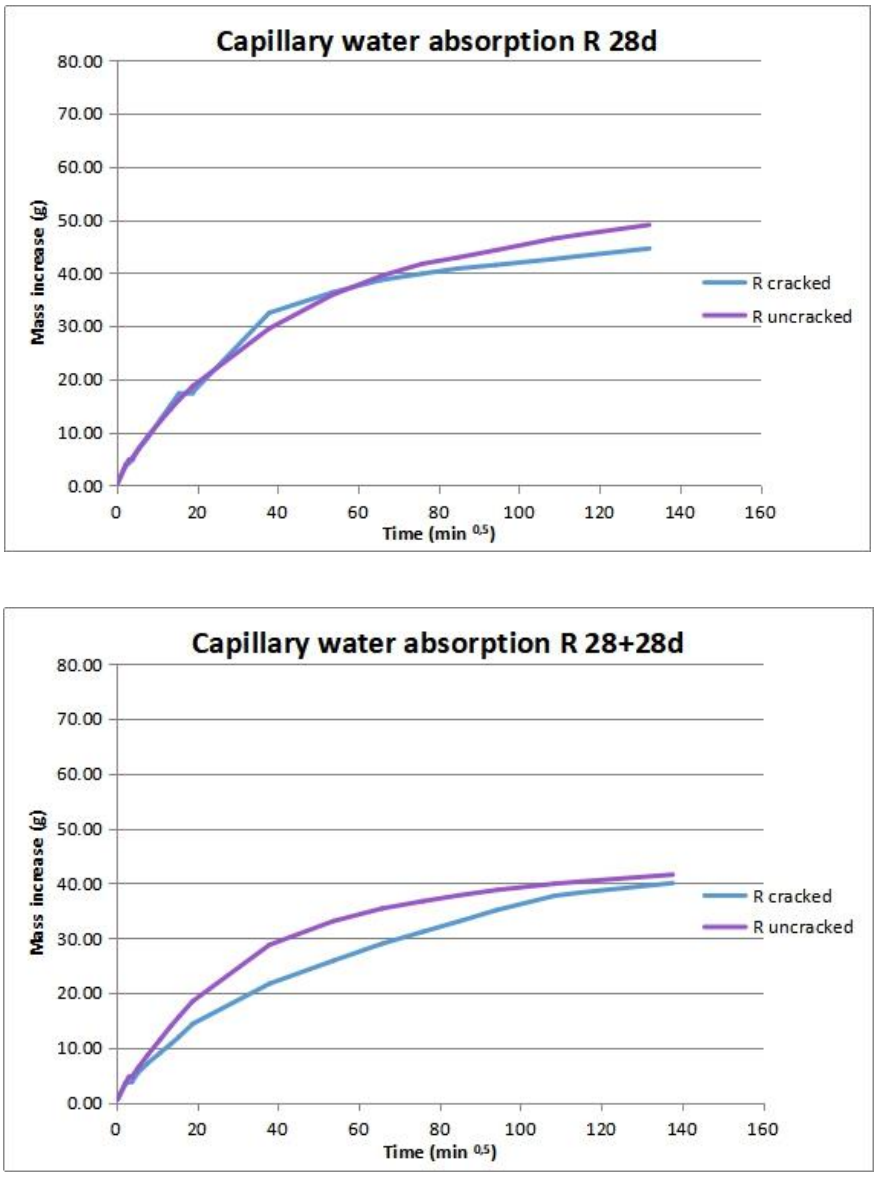

Figure 5.3. Mean mass increase of ECC reference specimens during the capillary water absorption test at 28d and 28+28d of healing

In the case of material A (figure 5.4), it is possible to observe a similar behaviour than in reference samples from 28d to 28+28d. At 28 d both types of specimens show the same initial mass increase rate, while an 8.8%higher final mass increase is observed in the case of cracked samples. In fact the values of the mean capillary absorption coefficient K are almost equal (0.1036 $kg/m^2min^{0.5}$ for uncracked and 0.1034 $kg/m^2min^{0.5}$ for cracked). This result suggest that cracks must be produced by the 3-point bending test at the inner part of the specimens and not at their surfaces.

At 28+28 days, cracked A samples show a slightly slower mass increase in the initial stages of the test possible because of the biomass ash which reduces spaces in samples The final mass increase is a 6.2% higher than for uncracked specimens, suggesting that a complete healing of cracks has not occurred during the 28 days after cracking. However, this difference, being slightly lower than the difference observed at 28 days, indicates that a partial healing of the cracks may have occurred. These results are in good agreement with the mechanical data of the specimens.

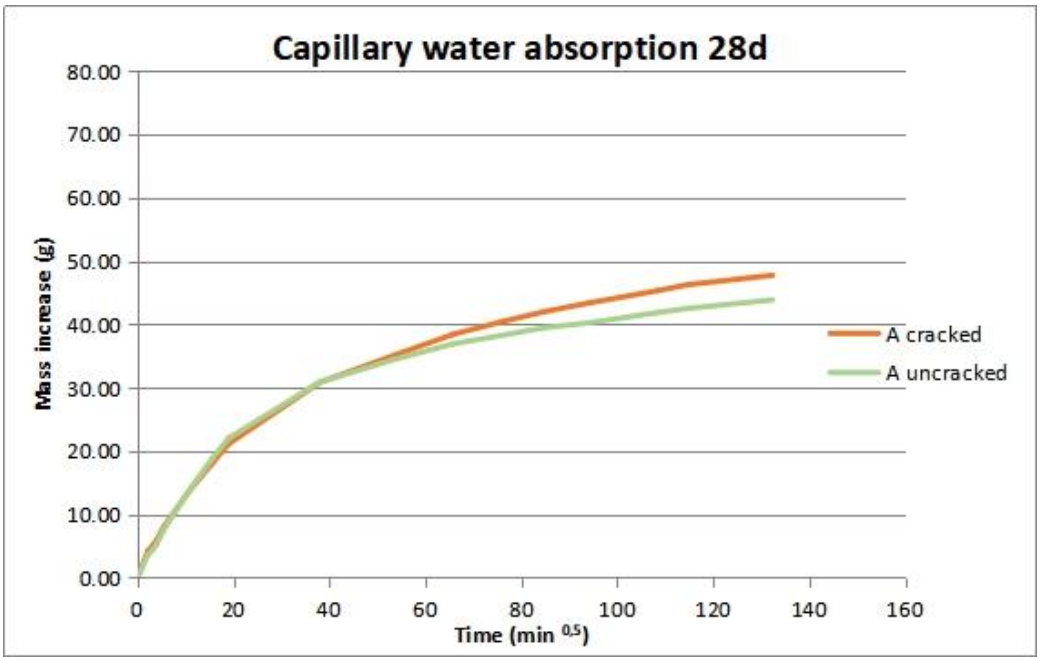

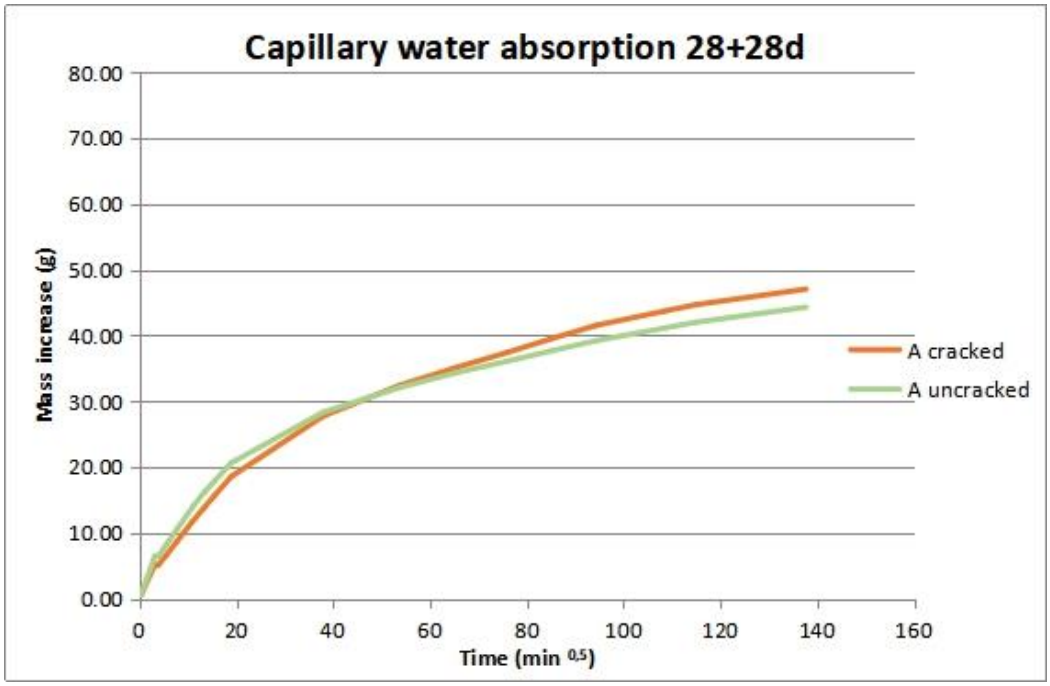

Figure 5.4. Mean mass increase of ECC specimens A during the capillary water absorption test at 28d and 28+28d of recovery

When a similar experiment was performed on sample B, there was no similarity in terms of rates of absorption between the cracked and uncracked samples at 28 days but rather, as might be expected, the cracked sample had a much higher absorption rate in addition to absorbing more water by the end of the experiment. In terms of the K coefficient, the value for uncracked sample is 0.072 $kg/m^2min^{0.5}$, significantly lower than material for A and R, and for cracked material B this value is higher, 0.1266 $kg/m^2min^{0.5}$. After 28+28 days, both cracked and uncracked specimens show a significant reduction in water intake rate in the first stages of the test and in the final total mass increase at the end due to an efficient densification of the composite upon hydration as can be observed in figure 5.4 and it is an expected behaviour.

Regarding the tightness recovery, the difference in mass increase curves between uncracked and cracked specimens clearly decreases after the 28 days of healing both in terms of their initial steepness and of the final mass increase. In fact, K value for cracked material decreases down to 0.1160 $kg/m^2min^{0.5.}$ and the final mass increase in cracked specimens is a 49.8% higher than in uncracked at 28 days, and only a 32.4% higher at 28+28d. These results could be an indicator that it is necessary to increase the recovery time in curing chamber beyond 28 days to further reduce the final mass increase and K value.

Comparing the behaviour of the two formulations implementing biomass ash, at both at 28d and 28+28d, material A shows a slower mass increase in the cracked sample, with a lower final mass increase value during the test than those of material B. These results suggest a higher density of the matrix in the composite A. However material B shows a much higher tightness recovery after 28 days of healing.

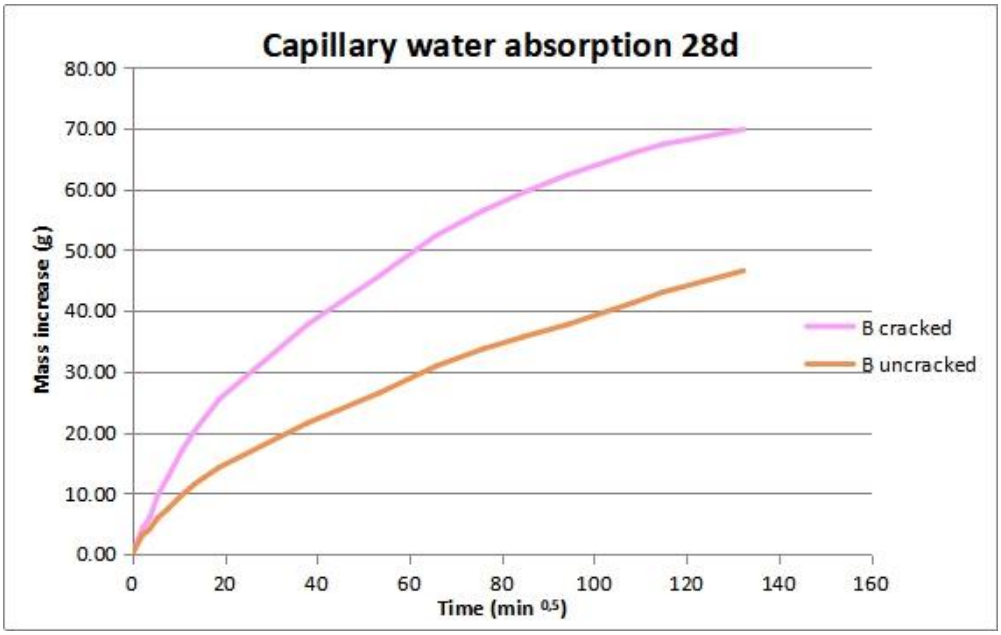

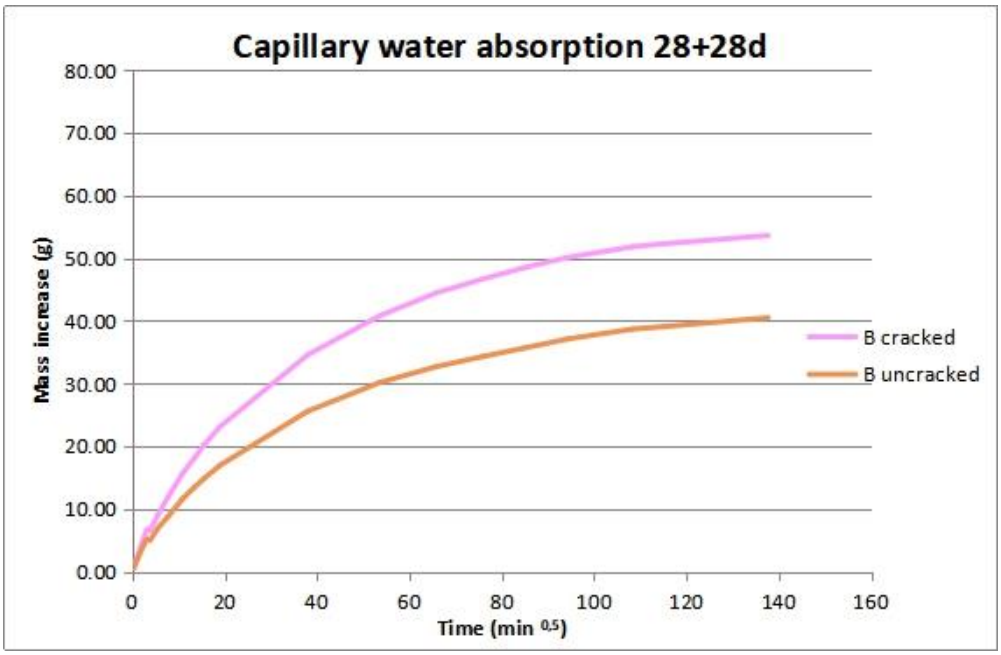

Figure 5.5. Mean mass increase of ECC specimens B during the capillary water absorption test at 28d and 28+28d of recovery

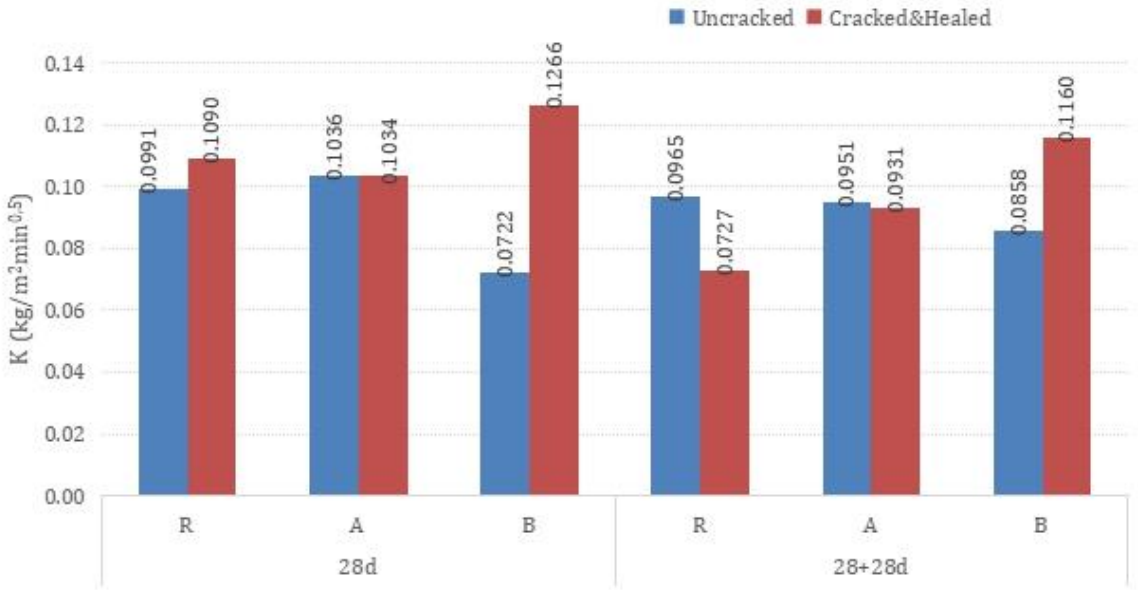

Figure 5.6. Capillary water absorption coefficient of the ECCs at 28d and 28+28d

5.2 Evaluation of the Chemical-Physical Properties of SCBM

5.2.1. Adsorption-desorption Isotherms. BET-N_2 Surface Area

Nitrogen adsorption tests were done on the cracked and uncracked samples in order to reveal how the microporosity and the BET-N_2 surface area have been modified by the presence of BA. All the samples (cracked and uncracked) showed characteristics of a type IV Isotherm as can be observed from gaphs in figure 5.7, where the isotherm has a slanted hysteresis loop with a clear separation between the end of monolayer and the beginning of multilayer adsorption. This is a typical behaviour when we are analyzing mesoporous materials (pore radius between 2-50nm).

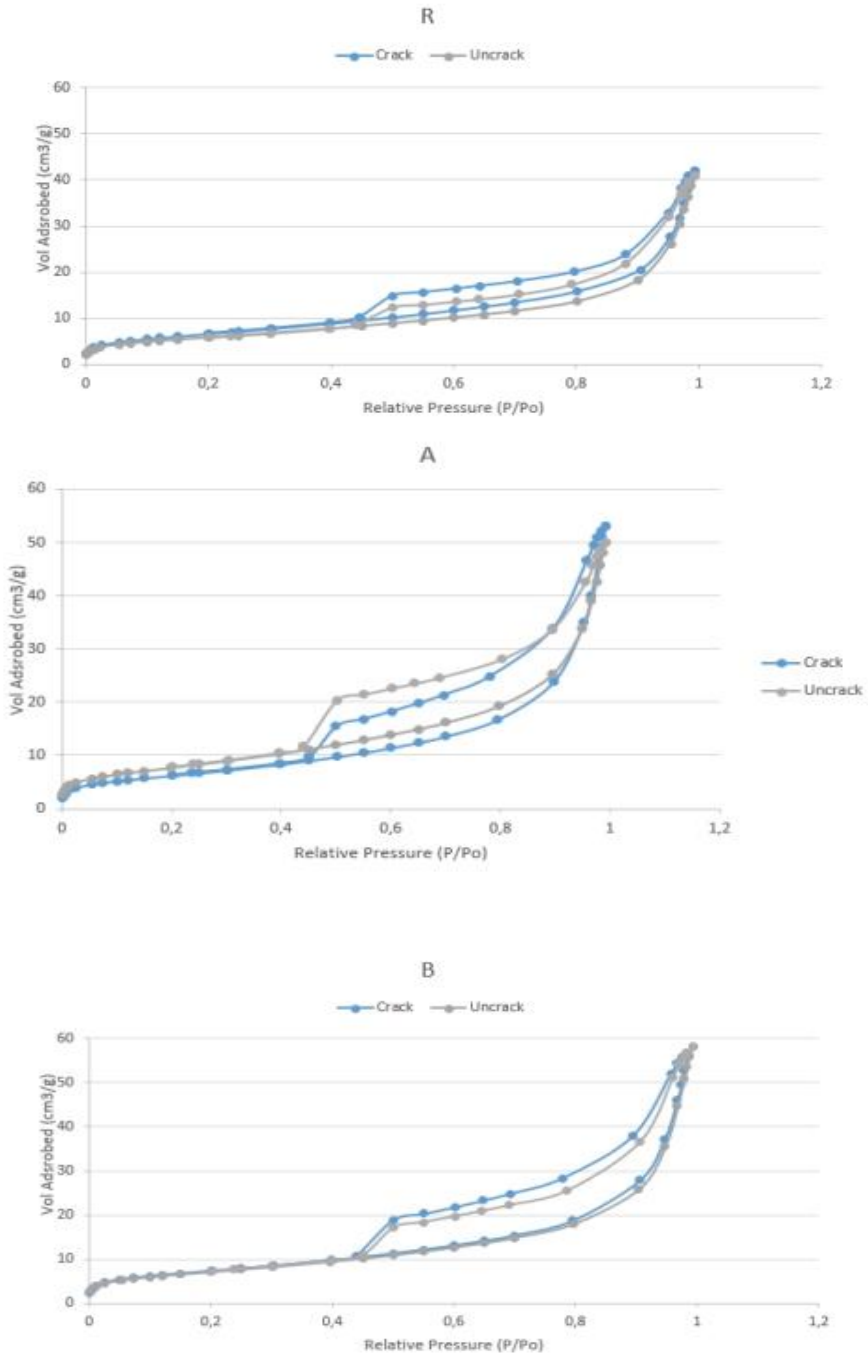

Figure 5.7. Graph showing relative pressure vs adsorbed volume in samples A and B and reference

The isotherms (figure 5.7) offer us additional information, which can corroborate the data given in the table 5.1 on BET-N_2 surface area and cumulative pore volume.

Table 5.1. Comparison of pore properties in ECC samples at 28 +28 days

Sample	BET-N_2 surface area (m^2/g)	Cumulative BJH pore volume (cm^3/g)
R uncracked	20.4718	0.059691
R cracked	23.9242	0.067591
A uncracked	27.5128	0.072816
A cracked	22.2219	0.078980
B uncracked	25.2009	0.086061
B cracked	25.9425	0.083481

The sample with a higher saturation (most adsorbed gas) point tends to have a larger surface area, comparative pore size can also be judged from these gaphs by looking at steepness of the isotherms, the steepest isotherm is from the sample with the largest pore size. Looking figure 5.7, the isotherm in B sample is steeper when the sample is uncracked, which is in ageement with the data in the table 5.1, it also absorbs more gas 58.19 cm^3/g at 0.993 relative pressure vs 55.89 cm^3/g at maximum of 0.976 relative pressure in the cracked sample. On the other hand, in sample A, the cracked specimen had the steepest isotherms as well as the higher adsorbed gas volume per gam, which is in total ageement with the data given before in the table 5.1. The cracked sample adsorbed 53.2 cm^3/g Nitrogen gas at 0.99 relative pressure whereas the uncracked sample reached 49.99 cm^3/g at 0.99 relative pressure. The reference sample offered similar behaviour to sample B, here the cracked sample was the one with the highest adsorption volume (42.1 cm^3/g at 0.99 relative pressure) compared to the uncracked sample (40.8 cm^3/g at 0.99 relative pressure)

The R samples and B sample showed an increase in BET surface area after developing cracks, where reference had 20.47 cm^2/g when it was not cracked against 23.92 cm^2/g after cracking, whereas B had 25.20 cm^2/g before cracks and 25.94 cm^2/g after. Sample A showed the exact opposite, the cracks decreased its BET surface area from 27.51cm^2/g when uncracked to 22.22cm^2/g afterwards. The average pore diameter offered a uniform behaviour across all samples, uncracked samples had higher values while cracked samples edged lower as illustrated in the table 5.1.

These results are useful to explain the modification of the microstructure in the sample. It is possible to stablish a good correlation between parameters of absorption-desorption isotherms and results of BET-N_2 surface area, that is, relative pressure (P/P_o) and $1/V_{ads}$ (P/P_o-1) (figure 5.8).

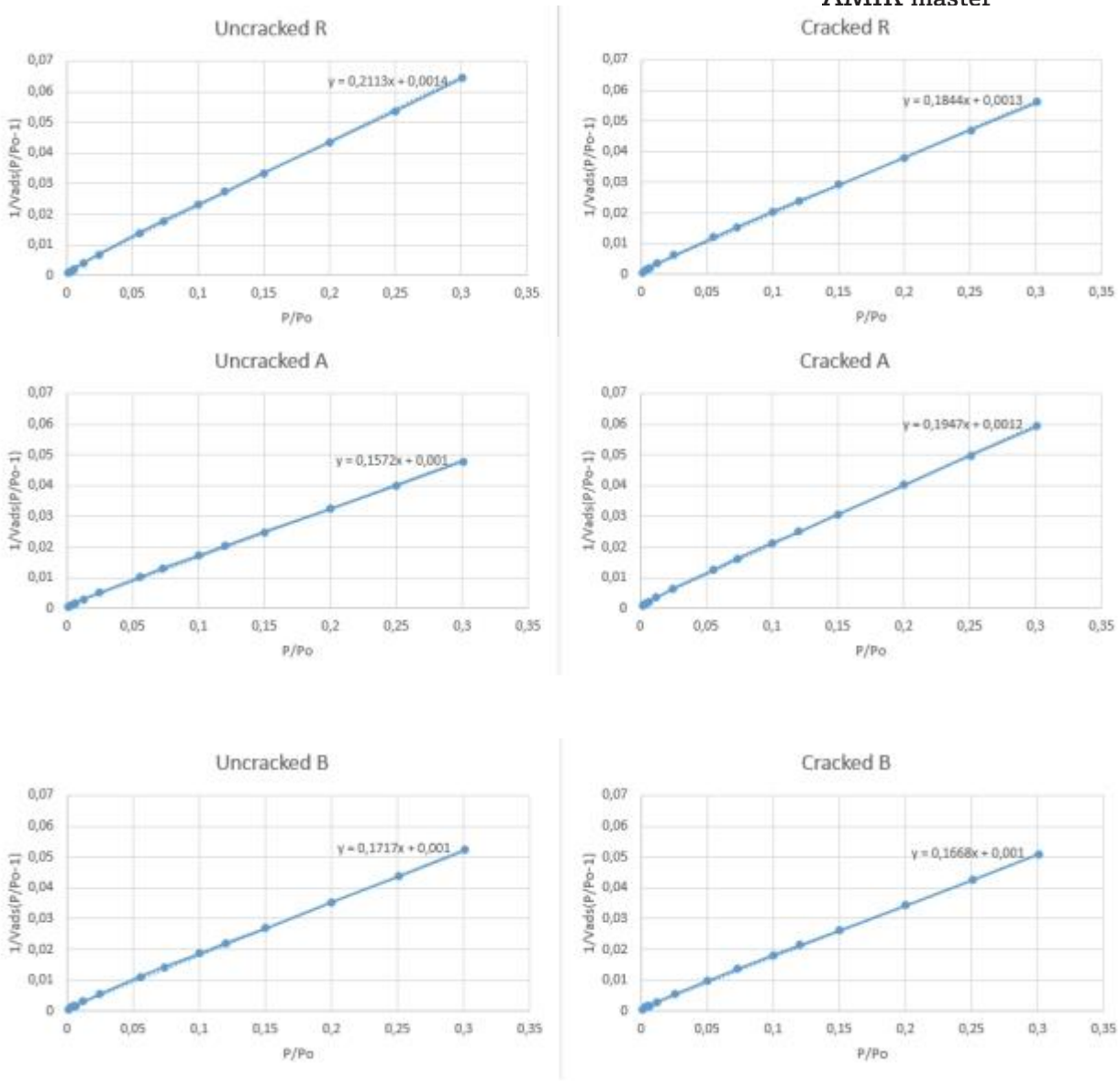

Figure 5.8. Correlation between parameters of absorption-desorption isotherms and results of BET-N_2 surface area

Another feature worth discussing is the pore size distribution (figure 5.9), i.e. the variation in pore diameters observed in samples before and after fracture. In samples A and B, there was formation of two clear peaks in the distribution (bi-modal) when the samples were cracked and cured for 28+28 days, the uncracked samples had wide distribution but with a main peak and a shoulder. The shoulder in uncracked B had higher intensity than uncracked. Guerrero et. al [26] attributed the presence of two peaks to the difference in density of the kind of C-S-H gels formed. The lower diameters at around 50 nm are likely due to gels. Uncracked samples A and B developed shoulders only without two intense peaks which we will also attribute to the density of C-S-H, the real difference comes when we compare A and B to R. The current hypothesis is that biomass rich samples end up with more calcite due to improved flow and entry of carbon dioxide in the cracks. There is an observable increase in pore volume which is directly correlating with the increased amount of biomass ash as can be seen in table 5.1.

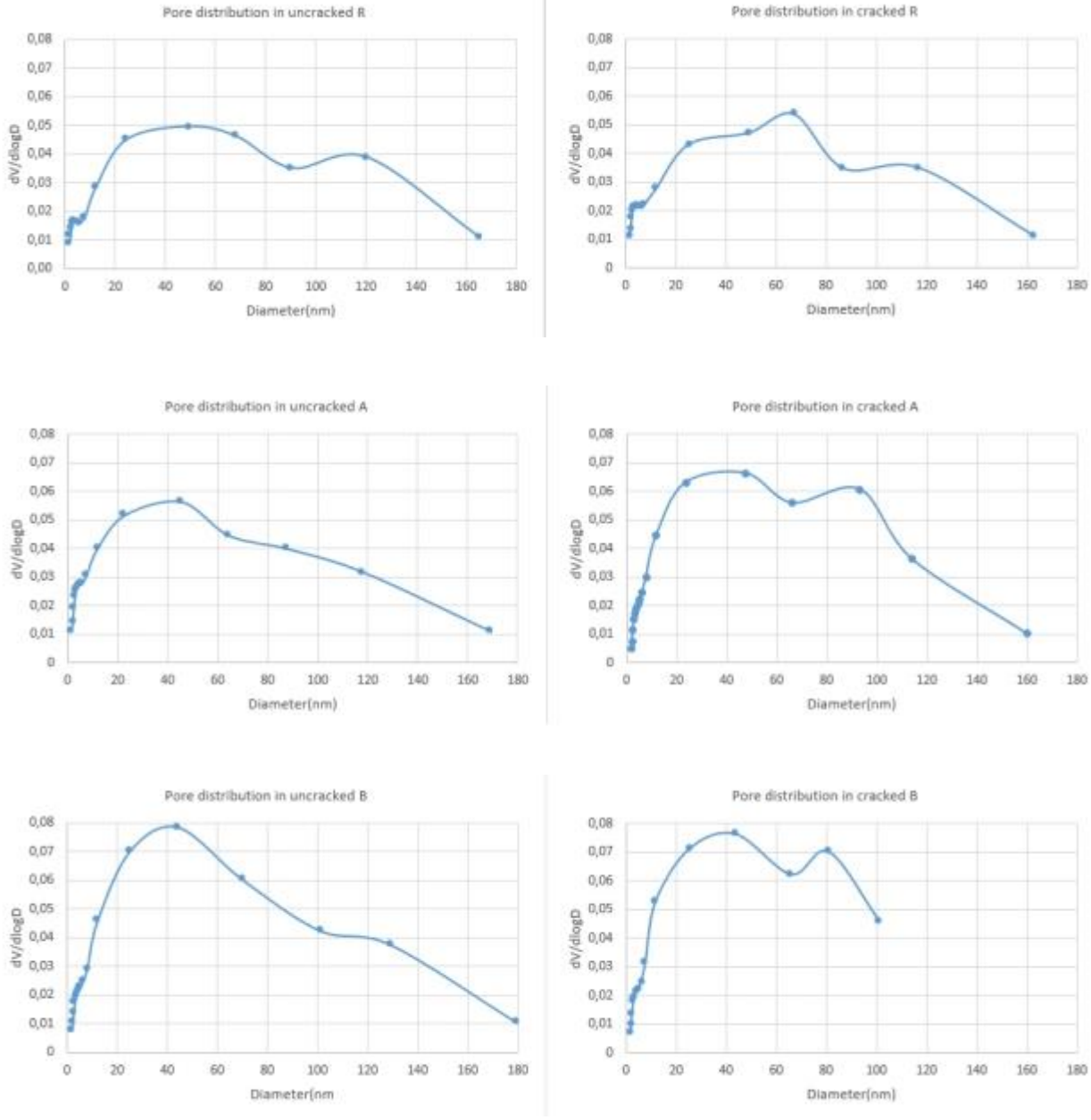

Figure 5.9. Pore size distribution for ECC samples (28+28 days)

5.2.2. Structural Characterization

X-Ray Diffraction

X-ray diffraction analysis was carried out in R, A and B samples, both uncracked and cracked, after 28d and 28+28d. Considering that the patterns are very similar in all cases, and taking into account that the principal aim of this work is to know the effect of BA in ECCs self-healing, only the results of 28+28d in R, A and B cracked materials are presented in figure 5.10. The main crystalline phases that can be found in ECCs at 28days are ettringite ($Ca_6Al_2(SO_4)_3(OH)_{12}(H_2O)_{26}$), Quartz ($SiO_2$), Portlandite ($Ca(OH)_2$) and Calcite($CaCO_3$).

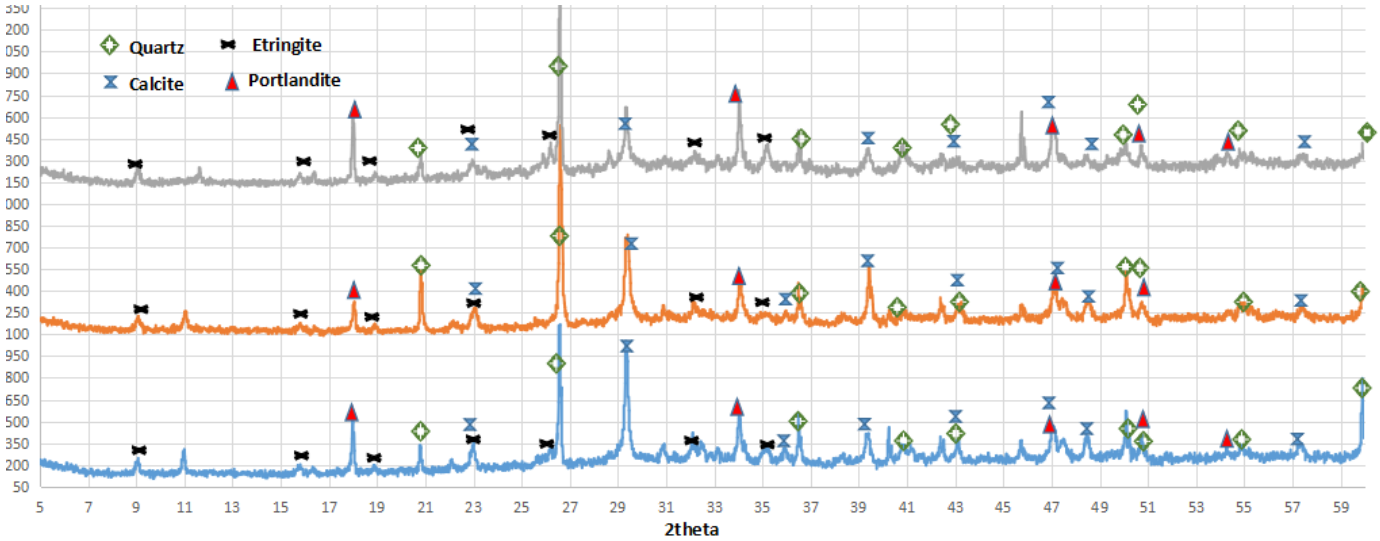

Figure 5.10. X ray diffraction of cured samples (28 +28 days)

The ettringite is a product of hydration in ordinary portland cements which is formed when tricalcium aluminate reacts with calcium sulfate, generally at lower or moderate relative concentrations of calcium sulfate.

$$3CaO{\cdot}Al_2O_3 + CaSO_4 \xrightarrow{(H2O)} (Ca_6Al_{2.}(SO_4)_3(OH)_{12}\,.\,(H_2O)_{26}) \qquad 18$$

It should be noted that a peak around 11 [2θ] appears in the patterns that is zoomed in figure 5.11. In the case of the reference sample, this peak can be attribute to the formation of calcium monosulfoaluminate (C_4ASH_{12}) as it is located at 11.6º [2θ]. However, for A and B samples, this peak appears around 11.0º [2θ] that corresponds to the formation of Friedel´s salt: $Ca_2Al(OH)_6(Cl){\cdot}2H_2O$, due to the presence of chloride ions in BA composition.

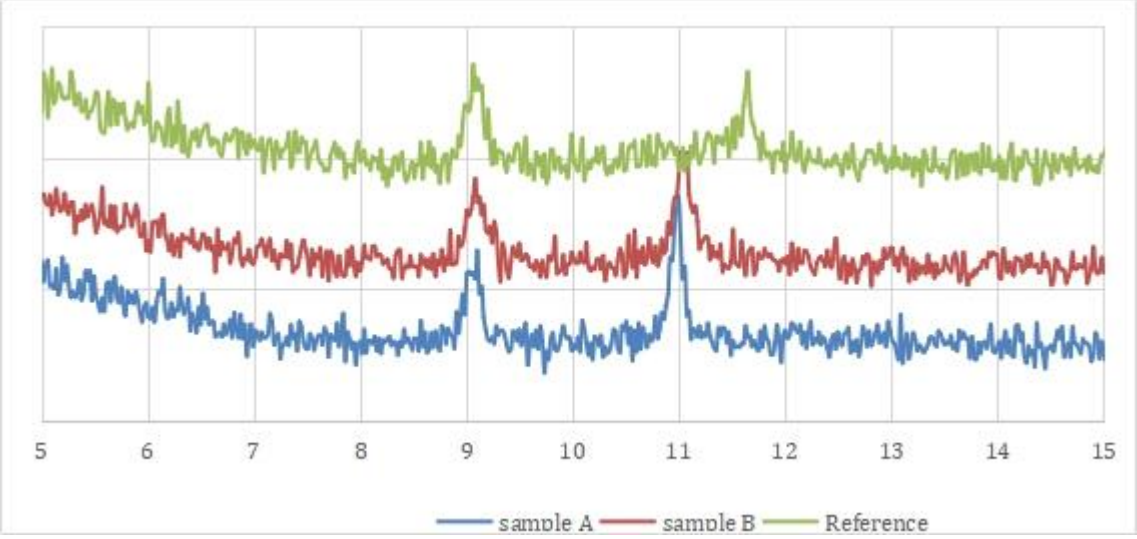

Figure 5.11. Zoomed of [2θ] equal to 11º of X ray diffraction of cured samples (28 +28 days)

Scanning Electron Microscopy (SEM) and dispersive energy analysis (EDX)

Figure 5.12 shows a general aspect of the R, A and B samples at 28d+28d, both uncracked and cracked. A good distribution of the PVA fibres can be observed in the matrix. Some cracks are observed in the R-uncraked case, probably due to the preparation of the samples.

In all cases there is a small porosity and homogeneous distribution of fly ash and biomass ash. These data are in accordance with the BET-N_2 surface area and pore volume commented previously.

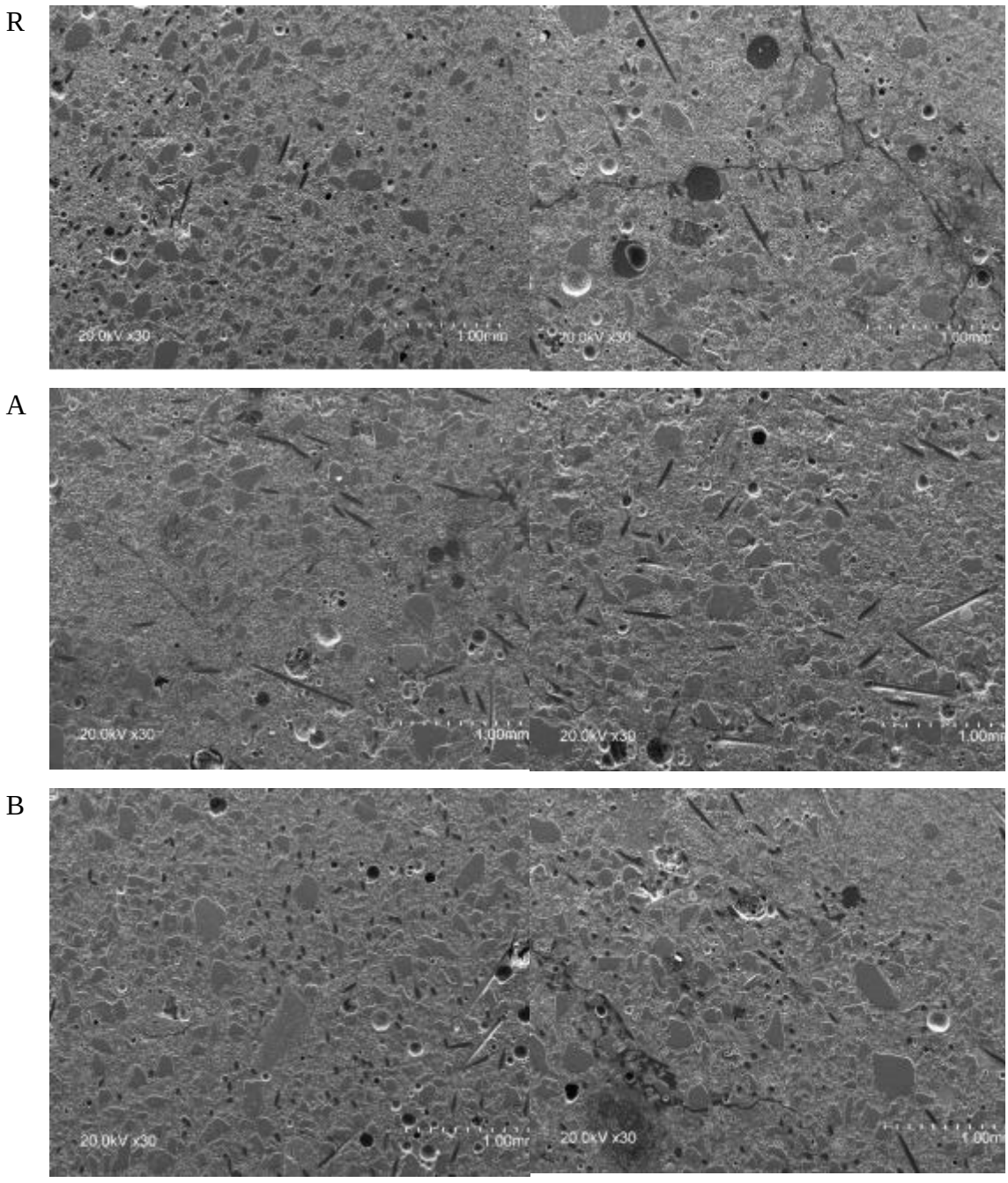

Figure 5.12. Scanning Electron Microscopy of Samples A, B and R

The analysis by scanning electron microscopy of the samples from the cracked area of material A, with lower content of BA, shows a compact microstructure where around the cracks the precipitation of calcium aluminosilicates appears (microanalysis 1 to 4 in figure 5.13) as hydration products formed during the recovery time in curing chamber.

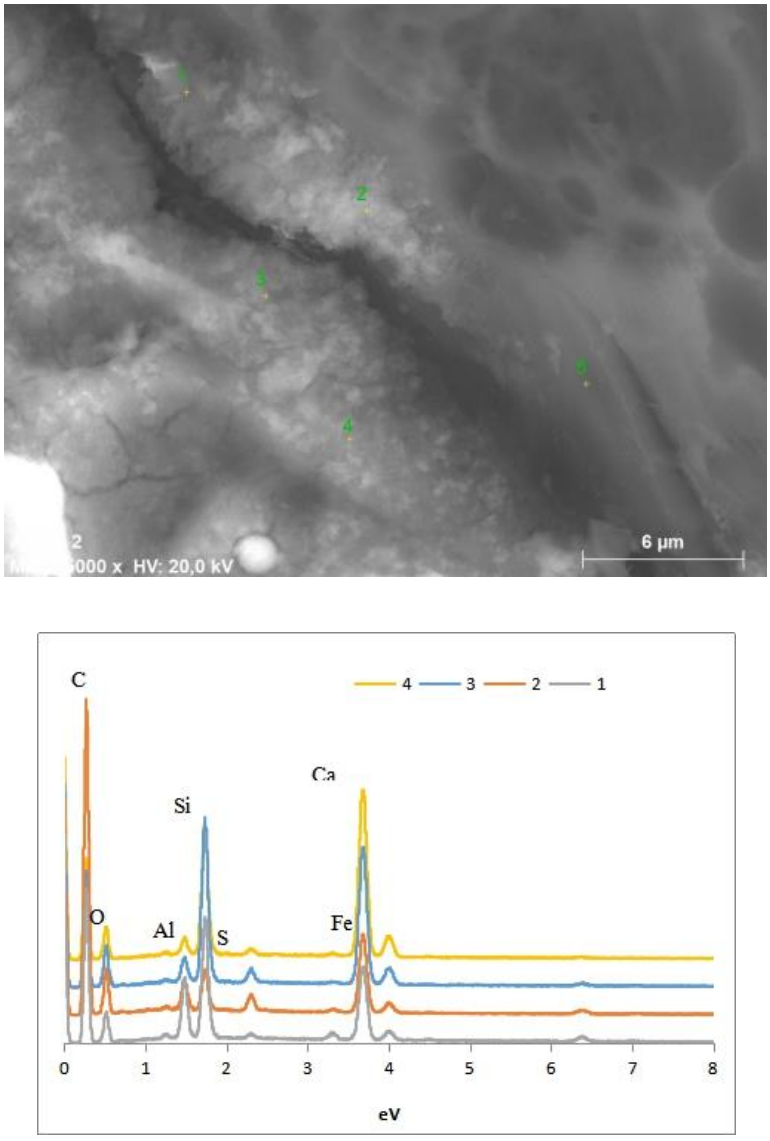

Figure 5.13. SEM-EDX results of cracked Sample A at 28+28d

Inside the microstructure, it is possible to distinguish a good interface of PVA fibres with the matrix; see the point marked with 5 in figure 5.13.

In the case of A sample uncracked (figure 5.14) a worst interface between PVA fibres (point 9) and the rest of the matrix is observed. Near the interface it appears the precipitation of calcium silicate hydrate (point 4) that may produce the mechanical behaviour observed in this sample (figure 5.2). In addition, we can observe different phases like Friedel Salt (point 8), mullite from fly ash (point 2, 3, 6) that confirm the results from X-ray diffraction analysis.

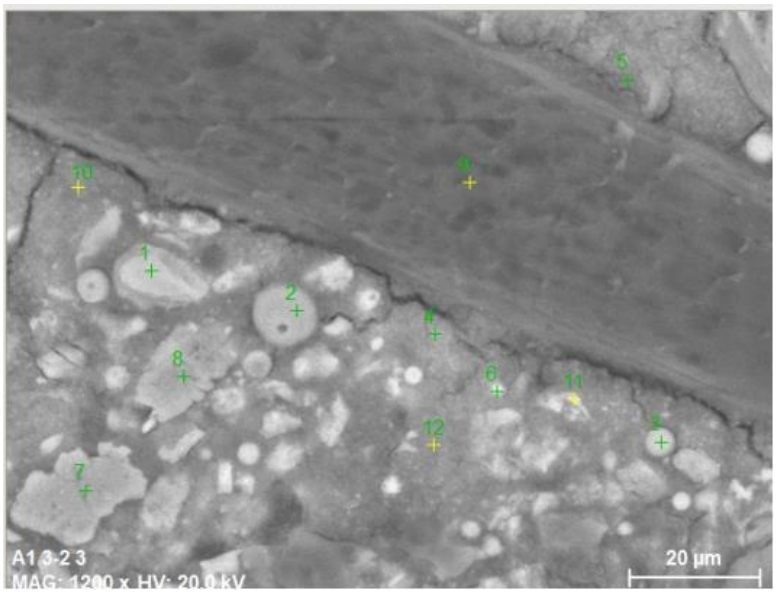

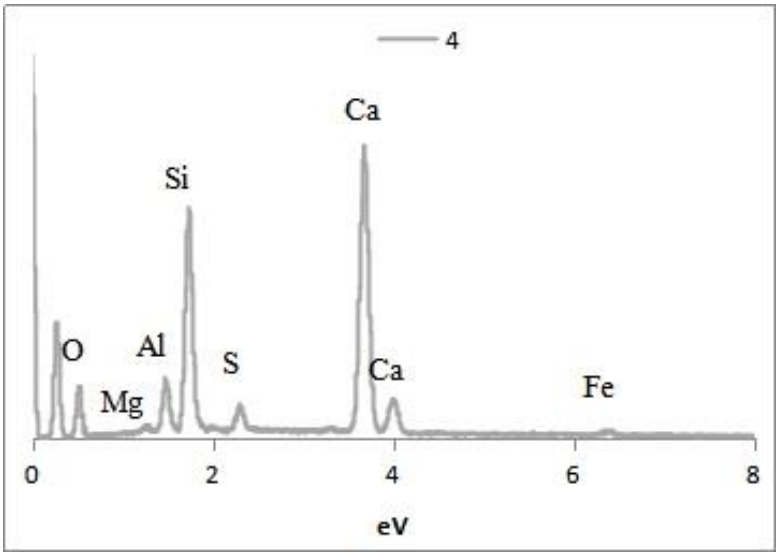
4
Ca
Si
O
Al
S
Ca
Mg
Fe
0
2
4
6
8
eV

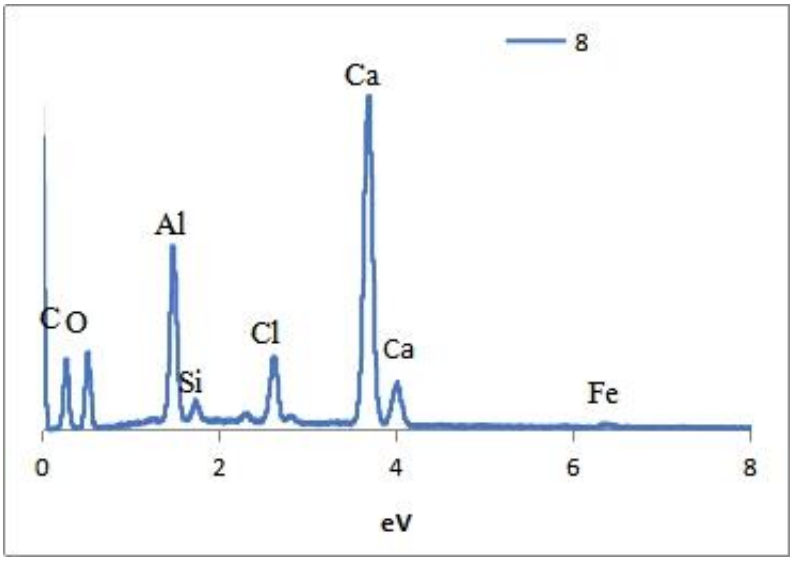
8
Ca
Al
C
O
Cl
Ca
Si
Fe
0
2
4
6
8
eV

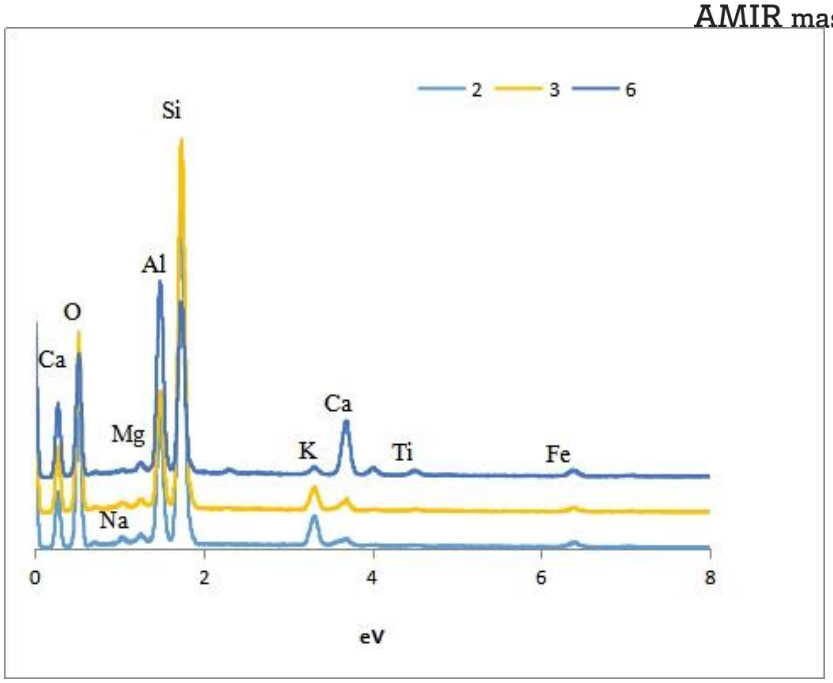

Figure 5.14. SEM-EDX results of uncracked Sample A at 28+28d

Figure 5.15 and 5.16 show the precipitation Friedel Salt (points 14, 19 and 34) in A samples, both cracked and uncracked, confined within pores but with void spaces that would permit the absorption of water by capillarity and thus avoid a total tightness recovery in this sample. This would also be consistent with the fact that, the recovery of mechanical strength is not total.

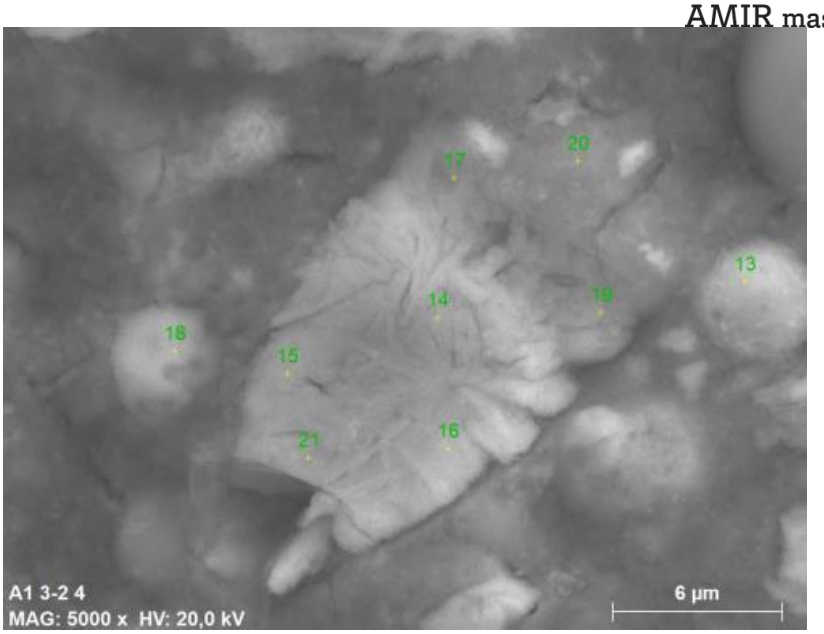

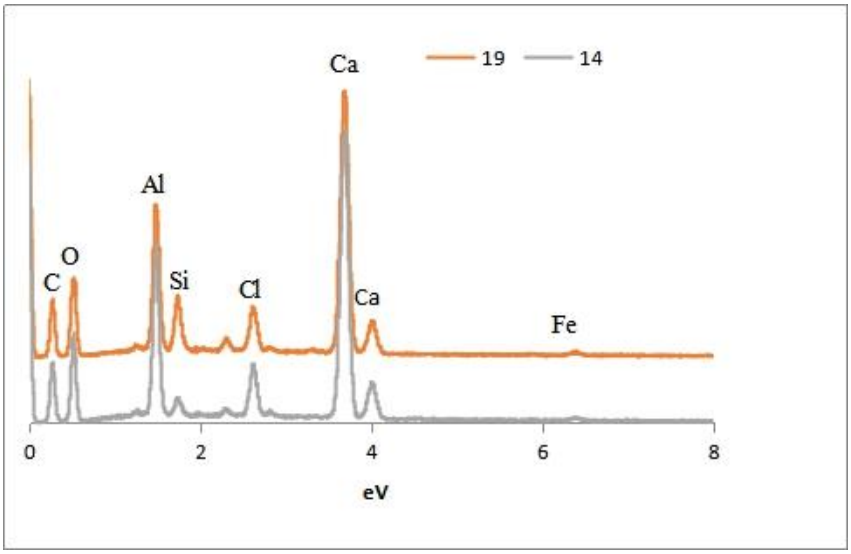

Figure 5.15. SEM-EDX results of Sample A at 28+28d: precipitation of Friedel salt

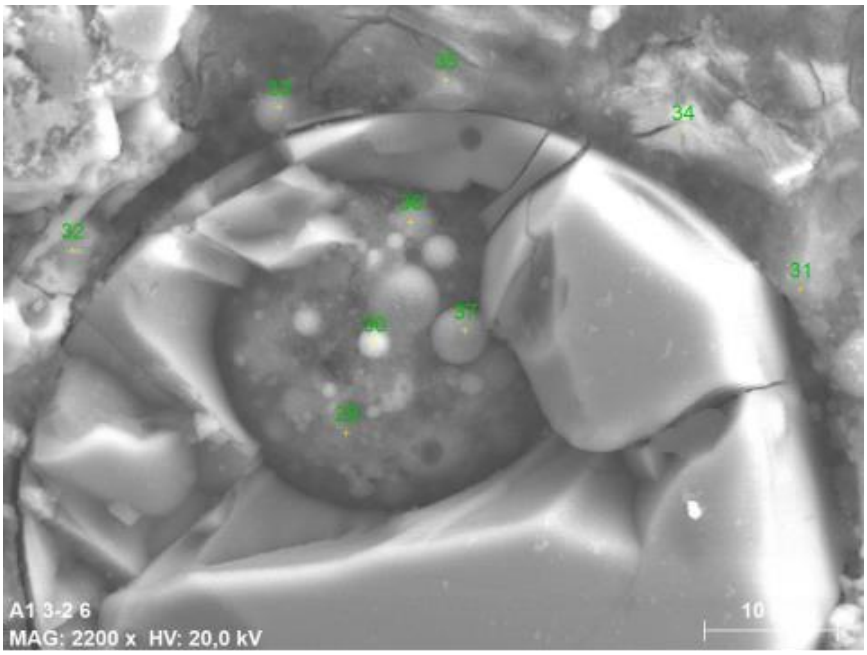

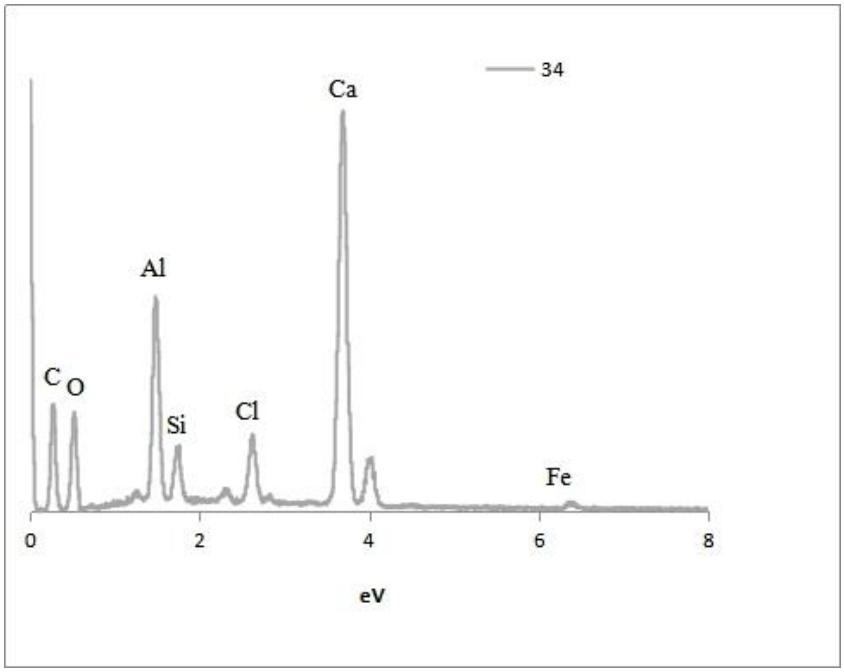

Figure 5.16. SEM and EDX analysis of sample A showing Friedel salts

Regarding cracked sample B at 28+28d, no broad open cracks can be observed along the surface of these samples (figures 5.17 and 5.18). These results suggest a high healing efficiency of the matrix when a higher content of biomass ash is used.

The detailed analysis of the crack in the case of ECC sample prepared with higher content of BA show healing products growing from both faces of the crack towards the middle, as observed in previous works by the authors Pérez et al [31]. The EDS analysis of points 31-34 show the precipitation of calcium silicates or calcium silicoaluminates, like C-S-H and C-A-S-H gels, that can close the crack. However, according to previous results, the presence of this hydration phases is insufficient to produce total recovery of transport properties in this materials (figure 5.5 and 5.6) but it is significant for mechanical strength recovery (figure 5.2) .

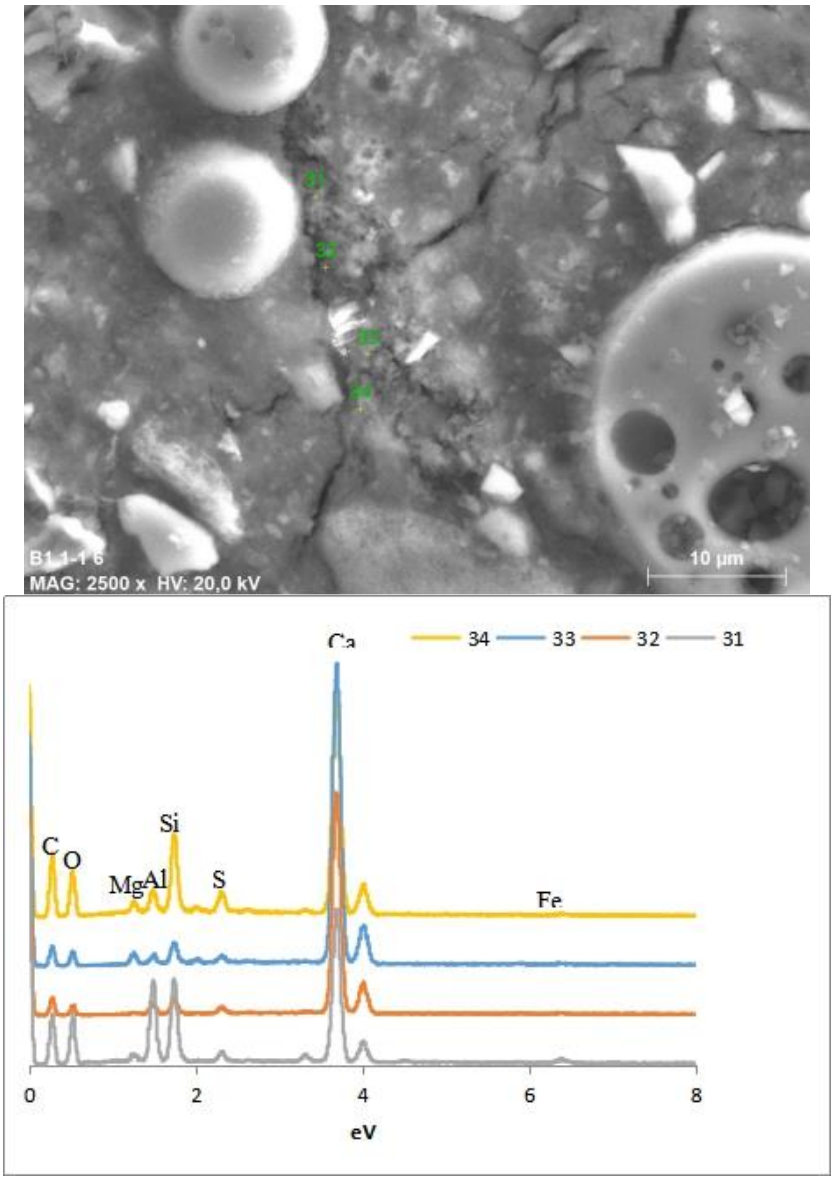

Figure 5.17. SEM-EDX results of Sample B at 28+28d

Together with the phases shown in the figure 5.18, a combination of sulphoaluminates and silicoaluminates of calcium precipitates are observed to seal others cracks within the sample B surface (figure 5.18. points 41 and 42). The microanalysis of points 41 and 42 indicates the precipitation of calcium silicoaluminates and Friedel salt in the area of cracks, which give rise to its sealing. However, given the expansive nature of Friedel's salt, the sealing is not as effective as it should be in terms of capillary data, where the capillary absorption coefficient is higher than in the uncracked sample 28+28d. However, the formation of hydration products around the cracks must account for the mechanical recovery, shown in Figure 5.2.

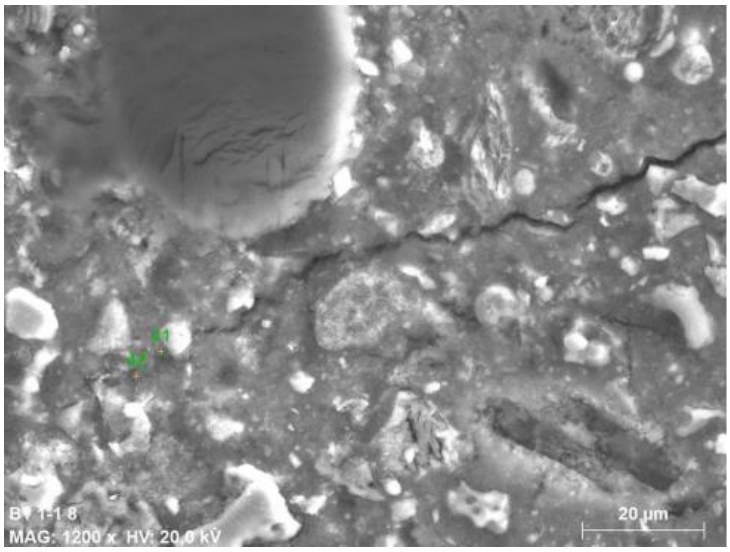

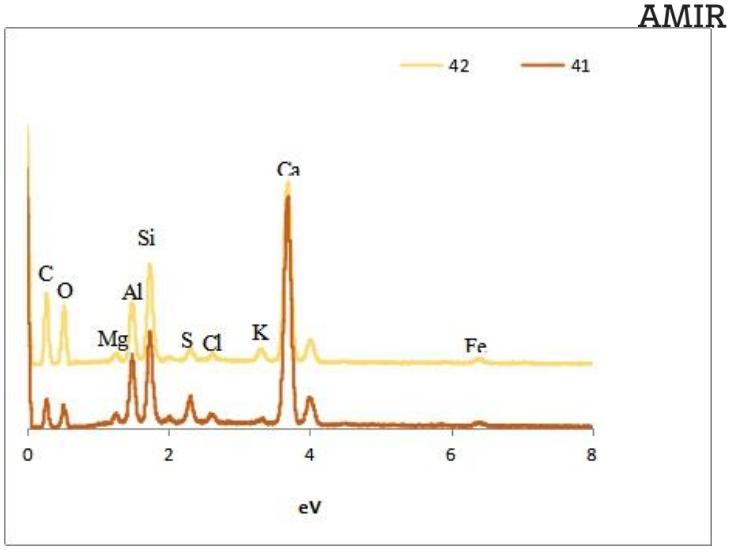

Figure 5.18 SEM-EDX results of Sample B at 28+28d

6. Conclusion

The samples were analyzed in order to understand the contribution provided by biomass ash towards the physical, mechanical as well as chemical properties of the mortars. The following are the key takeaways in this research:

- Mechanically, biomass improved the initial performance of the samples when flexural and compressive test were performed, samples A and B had better properties at 28 days; Reference started with 8.9 MPa flexural strength, A had 10.21 MPa and B had 9.58 MPa. The reduction of fly ash in samples A and B means reduced late stage strength improvement, since fly ash reacts slowly so at 28+28 days while pristine samples A and B had higher flexural strength (10.78 MPa for A and 10.74 MPa for B). The reference showed the most improvement by going from 8.9 to 9.63 MPa over a 28 day period.

-For 28+28 days healing, the reference was the sample with higher flexural resistance recovery (9.63 MPa pristine vs 9.42 MPa cracked and healed), sample B was not too far in it srecover its pristine sample at 28+28 days had 10.73MPa while the cracked and healed sample had 8.95 MPa which is interestingly closer to values observed in reference.

-All samples showed a reduction for water absorbed these points to formation of hydration and pozzolanic reaction products, which fill up the cracks. Sample B absorbed the most water when cracked, although there is also a considerable drop for water absorbed in both cracked B and uncracked samples at the end of 28+28 days. By comparing this data to the one found in adsorption analysis we find that both sample B simply had bigger accumulative BJH pore volume both as cracked and uncracked samples.

This work has shown that it is possible to replace fly ash with biomass ash when self-healing capability is the criteria, although a much wider investigation would be required to understand long-term effects of the changes.

7. Future work

There is a need to understand the kinetic influence of the biomass ash waste in the concrete especially towards the formation of C-S-H compounds, perhaps a binary experiment where only the ash and cement are researched to see the kind of microstructures they will form. The other facet that has to be explored is material processing, biomass ash containing samples were observed to have a higher need for water for the same viscosity observed in reference.

Lastly the optimization of material performance has to be explored via the understanding of proper stoichiometry, as well as the relationship between a biomass' matrix and fibres.

References

[1] V. Li, S. Wang, and C. Wu "Tensile Strain-Hardening Behaviour of PVA-ECC". ACI Materials Journal vol. 98, pp 483–492, 2001

[2] M. Li, and V. Li,. "Cracking and Healing of Engineered Cementitious Composites under Chloride Environment". ACI Materials Journal vol. 108, Tech. paper, Title no. 108-M36, 2012

[3] P. Bo, Z. Zhou, P. Hou, P. Du, Z. Lina and H. Xu. "Autogenous and engineered healing mechanisms of carbonated steel slag aggregate in concrete". Construction and Building Materials vol. 107, pp 191-202 , 2016

[4] ASTM International, "Standard Specification for Coal Fly Ash and Raw or Calcined Natural Pozzolan for Use in Concrete", *ASTM International* C618-05, 2005. [Online]. Available: https://www.astm.org/DATABASE.CART/HISTORICAL/C618-05.htm [accessed 15/06/2019].

[5] Energy Information Admistration, "Energy from municipal solid waste", *Energy Information Admistration,* 2019. [Online]. Available: https://www.eia.gov/energyexplained/?page=biomass_waste_to_energy , [Accessed: 12/06/2019].

[6] R. Gunti, P. Ratna, and A. Gupta, "Mechanical and degradation properties of successive alkali treated completely biodegradable sisal fibre reinforced poly lactic acid composites". Journal of Reinforced Plastics and Composites, vol. 34. 10, 2015

[7] E. Yang, S. Wang, Y. Yang, and V. Li, "Fibre-Bridging Constitutive Law of Engineered Cementitious Composites", Journal of Advanced Concrete Technology, Vol. 6, pp 181-193, 2002

[8] Y, Weng, B. Lu, J. Ming, M.J. Tan and S. Qian, " Rheology and Printability of Engineered Cementitious Composites-A Literature Review", Proceedings of the 2nd International Conference on Progress in Additive Manufacturing (Pro-AM 2016),Singapore, 2016

[9] H. Wu, and V. Li, "Snubbing and Bundling Effects on Multiple Crack Spacing of Discontinuous Random Fibre-Reinforced Brittle Matrix Composites". Journal of the American Ceramic Society, Vol. 75, pp 3487 - 3489. 1992

[10] V. Li, "Post-Crack Scaling Relations for Fibre-Reinforced Cementitious Composites", Journal of Materials in Civil Engineering - J MATER CIVIL ENG, Vol.4 (1), pp 41-57, 1992

[11] Z. Lin, and V. Li, "Crack Bridging in Fibre Reinforced Cementitious Composites with Slip-hardening Interfaces", Journal of the Mechanics and Physics of Solids, Vol.45, pp 763-787 .1997

[12] S. Wang, and Li, Victor, "Engineered Cementitious Composites with High-volume Fly Ash". ACI Materials Journal, Vol. 104, pp 233-241, 2007

[13] M. Şahmaran, and V. Li, "Durability properties of micro-cracked ECC containing high

volumes fly ash", Cement and Concrete Research, Vol. 39. 1033-1043, 2009

[14] D. M. Lepech, V. Li, E. Robertson, A. Richard, and G. Keoleian, " Design of Green Engineered Cementitious Composites for Improved Sustainability", ACI Materials Journal. Vol. 105(6), 2011

[15] R.M. Salvo, C. Stefano, M. Novajra, C. Giorgia , B. Fulvio,and M. Ferrari "Biomass ash as supplementary cementitious material (SCM)", Advances in Applied Ceramics, Vol. 114, 2015

[16] R. Teixeira, G.H.D Tonoli, S. Santos, S. Rayon, E. Amigó, V. Jr and R. Holmer " Nanoindentation study of the interfacial zone between cellulose fibre and cement matrix in extruded composites", Cement and Concrete Composites Vol.85,2017

[17] N Kumar ,K Patil ,Rayna Higuchi ,David P. Ferrell ,Vanya A. Luttrull , & Joan G. Lynam "Use of Biomass Ash for Development of Engineered Cementitious Binders", ACS Sustainable Chem. Eng. Vol.6, p 10, 2018

[18] C.K. Park, M.H. Noh and T.H. Park, "Rheological properties of cementitious materials containing mineral admixtures" Cement and Concrete Research, Vol. 35, pp842-849 , 2004

[19] M. Li, and V. Li, "Rheology, fibre dispersion, and robust properties of Engineered Cementitious Composites", Materials and Structures, Vol. 46(3), 405-420, 2013

[20] K. Tittelboom and N. De Belie, "Self-Healing in Cementitious Materials—A Review", Materials,Vol. 6, pp2182-2217, 2013

[21] V. Li, Yang, and E.-H "Self-Healing in Concrete Materials", Self-Healing Materials: An Alternative Approach to 20 Centuries of Materials Science, Springer, pp161-193, 2007.

[22] N. Hearn and C.T. Morley," Self-healing property of concrete–Experimental evidence", Mater. Struct.Vol. 30 (7), pp404–411,1997

[23] C. Weben, W.S. Smith, and M.W. Wardle, "Test methods for fibre tensile strength, composite flexural modulus and properties of fabric-reinforced laminates", Composite Materials: Testing and Design, 5th Conference, ASTM International,1979

[24] V. Zhang, and, H. , *Cement Building Materials in Civil Engineering*, Woodhead Publishing ,Philadelphia, pp46–423,2011

[25] C. Hall, "Water sorptivity of mortars and concretes: a review", Magazine of Concrete Research, Vol.41(147), pp 51–61, 1989

[26] K.S.W. Sing, D.H. Everett, R.A.W. Haul, L.Moscou, R.A. Pierotti, J. Rouquerol, and T. Siemieniewska, T. *Pure Appl. Chem.* Vol. 57, pp 603. 1985

[27] G. Pirngruber, "Characterization of porous solids - Characterization of Catalysts and Surfaces", Jan. 25, 2016. [Online].Available: https://www.ethz.ch/content/dam/ethz/special-interest/chab/icb/van-bokhoven-group-dam/coursework/Characterization-Techniques/2016/physisorption-pore-size-analysis-2016.pdf. [Accessed: May 30, 2019].

[28] R. Rajamma,D. Soares, T.C. Esteves, S.Santos,J.A. Labrincha and V.Ferreira, "Investigation of Alkali-Silica Reaction in Concretes with Biomass Fly Ash", Construction and Building Materials Vol. 26(1) pp 687–693 , 2012

[29] V. Li, and E. Yang, "Engineered self-healing cementitious composites", Patent US20080261027A1, Aug. 2009.

[30] A. Guerrero, S. Goni, J.S Dolado "Belite Cements: Modification of calcium Silicate Hydrate (C-S-H) gel by alkaline hydrothermal activation" ACI Materials Journal Vol.106(2),

2009
[31] G. Perez, G. Calvo. , C. Pedro and A. Guerrero "SynerCrete'18 International Conference on Interdisciplinary Approaches for Cement-based Materials and Structural Concrete", Presented at Funchal, Madeira Island, Portugal, 2018.
[32] R. Sumrerng, and P. Chindaprasirt, "Use of Rice Husk-Bark Ash in Producing Self-Compacting Concrete", Advances in Civil Engineering. Vol. 2 , Pp 1-6 , 2014

LIST OF FIGURES

LIST OF TABLES